Top Curr Chem (Z) (2017)375:12
DOI 10.1007/s41061-016-0100-9

REVIEW

Nanostructured Materials Synthesis Using Ultrasound

Jordan J. Hinman[1] · **Kenneth S. Suslick**[1]

Received: 11 November 2016 / Accepted: 21 December 2016
© Springer International Publishing Switzerland 2017

Abstract Recent applications of ultrasound to the production of nanostructured materials are reviewed. Sonochemistry permits the production of novel materials or provides a route to known materials without the need for high bulk temperatures, pressures, or long reaction times. Both chemical and physical phenomena associated with high-intensity ultrasound are responsible for the production or modification of nanomaterials. Most notable are the consequences of acoustic cavitation: the formation, growth, and implosive collapse of bubbles, and can be categorized as primary sonochemistry (gas-phase chemistry occurring inside collapsing bubbles), secondary sonochemistry (solution-phase chemistry occurring outside the bubbles), and physical modifications (caused by high-speed jets, shockwaves, or inter-particle collisions in slurries).

Keywords Sonochemistry · Nanomaterials · Microspheres · Nanoparticles · Ultrasonic

1 Introduction

The production of nanostructured materials through the effects of high-intensity ultrasonic irradiation of materials has been a subject of interest for more than two decades [1–5]. The ultrasonic irradiation of a liquid can cause effects over a large range of size scales, from the mixing and heating of the bulk liquid to the concentration of energy in microscopic hot spots intense enough to produce high-energy chemical

This article is part of the Topical Collection "Sonochemistry: From basic principles to innovative applications"; edited by Juan Carlos Colmenares Q., Gregory Chatel.

✉ Kenneth S. Suslick
ksuslick@illinois.edu

[1] Department of Chemistry, University of Illinois at Urbana-Champaign, 600 S. Mathews Av., Urbana, IL 61801, USA

Published online: 11 January 2017

reactions. Both the physical and chemical effects of ultrasound have been utilized in the production of nanostructured materials. The complex and wide range of processes caused by ultrasound—both chemical and physical—provides a diverse palette for the formation nanomaterials with a variety of compositions and structures.

The chemical effects of ultrasonic irradiation in a liquid are not the result of direct coupling of the sound waves to molecular species, as they occupy very different time and length scales. Rather, sonochemistry arises as a consequence of the implosive collapse of bubbles produced by acoustic cavitations [6]. The process of nucleation, growth, and collapse of bubbles during acoustic cavitation is shown graphically in Fig. 1. When a liquid is subject to sufficiently strong acoustic waves, dissolved gases or other impurities nucleate cavities (bubbles) within the liquid during rarefaction. Through successive cycles, the cavities grow through rectified diffusion—the decrease in cavity volume during compression is less than the growth during rarefaction due to the reduced surface area of the bubble during compression. When the bubble reaches a certain size (microns for 20-kHz ultrasonic irradiation) it becomes resonant with the ultrasonic radiation and can rapidly increase in size. Soon the bubble becomes unstable and violently collapses, producing a hot spot within the liquid medium [7].

Spectroscopic studies of the light emitted during cavitation (i.e., sonoluminescence) by Suslick et al. have shown that these implosions generate conditions of 5000 K and 1000 bar in clouds of cavitating bubbles and even more extreme conditions in isolated single bubble cavitation [6, 8–11]. It is within these regions of extreme conditions that chemical reactions occur. Suslick et al. also studied the rate of ligand substitution for metal carbonyl sonolysis as a function of metal carbonyl vapor pressure and found the sonochemical reactions must be taking place in two regions—gas phase and liquid phase [7, 12]. The liquid phase is mostly composed of droplets injected into collapsing bubbles [12], and perhaps a thin shell surrounding the collapsing bubble. Temperatures of the two sonochemical regions in low vapor pressure alkanes were determined to be 5200 and 1900 K for the gas

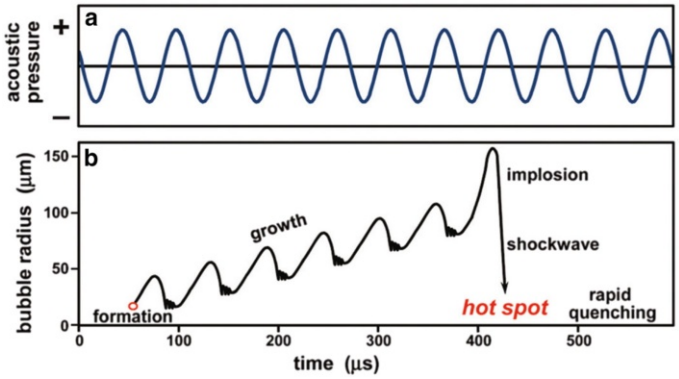

Fig. 1 Graphical representation of the growth and collapse of acoustic cavitation bubbles. As a liquid is irradiated with ultrasound, it is subjected to periodic compression and rarefaction (**a**). Bubbles formed in the liquid undergo expansion and compression and the size of the bubble oscillates until resonance occurs and implosive collapse follows (**b**). Reproduced with permission from Ref. [1]. Copyright 2012 Royal Society of Chemistry

phase and liquid phase, respectively. The extremely short lifetimes of cavitation events results in heating and cooling rates of more than 10^{10} K s^{-1} [6, 12]. As shown in Fig. 2, the conditions of sonochemistry are quite extreme in comparison to other chemical processes.

This review will focus on recent examples of the use of ultrasound for the synthesis of nanostructured materials and will be organized according to the mechanisms by which ultrasound can be used for the production of nanomaterials. Section 2 focuses on nanomaterials produced using the chemical effects of ultrasound, and this section is further divided by the use of primary sonochemistry or secondary sonochemistry. In Sect. 3, various methods for using the physical processes of ultrasound to create nanostructured materials are explored. This section is subdivided into (1) ultrasonic spray techniques to generate microdroplet reactors for the generation of nanostructured materials; (2) sonofragmentation and sonocrystallization; and (3) sonochemically produced protein microspheres, which are created by a combination of chemical and physical effects.

2 Chemical Effects of Ultrasound

As a result of the extreme conditions during cavitation bubble collapse, both physical and chemical processes are initiated. The implosive collapse of bubbles generates a shock wave that propagates out into the liquid medium. Bubble collapse near a solid surface disrupts the spherical symmetry of the bubble and causes the formation of microjets that can impact the surface in addition to the shock wave. These physical processes make ultrasonic irradiation an effective means to mix

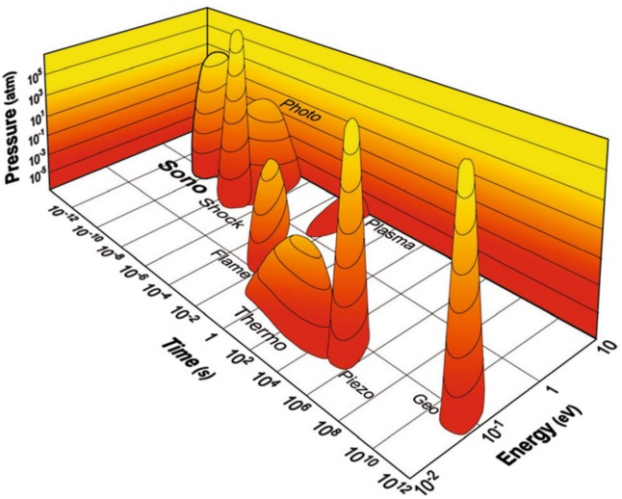

Fig. 2 Graph showing the "islands of chemistry", a graphical comparison of the timescale, energy, and pressure of various chemical processes. As shown in the graph, sonochemistry is a comparatively fast, high-energy, and high-pressure process. These conditions allow for the sonochemical production of various materials. Reproduced with permission from Ref. [1]. Copyright 2012 Royal Society of Chemistry

liquids, erode solid surfaces, and facilitate interparticle collisions. Of course, another consequence of ultrasonic irradiation is the eventual bulk heating of the solution; with typical ultrasonic horns, ultrasonic intensities are ~ 50 W cm^{-1}, such bulk heating can be significant in small liquid volumes.

Figure 3 provides a general scheme of the applications of sonochemical and ultrasonic processes to materials chemistry.

The chemical effects of ultrasound mostly derive from the hot spots created by collapsing bubbles. The effective compressional heating generates local temperatures high enough to cause the dissociation of all chemical bonds (up to and including N_2) [13]. Volatiles and gases present inside the collapsing bubble can undergo reaction and we refer to these as primary sonochemical reactions. Secondary sonochemical reactions occur involving these initially formed species after they have migrated into the surrounding liquid. Many radical species that will be formed within an ultrasonic hot spot can undergo a variety of secondary reactions with solutes in the surrounding liquid [14].

In the case where water is the sonicated liquid, sonolysis of water will generate highly reactive hydrogen atoms and hydroxyl radicals, and upon diffusion out of the hot spot, these species can initiate secondary sonochemical reactions (e.g., reductions, oxidation, hydroxylation of organics, etc.). The sonolysis of water is a well-studied process [15] and involves a number of rapid primary and secondary reactions that can also involve dissolved gases (e.g., O_2), as shown below.

$$
\begin{aligned}
&H_2O\ -))) \rightarrow\ H^{\cdot} + {}^{\cdot}OH\ ,\\
&H^{\cdot} + H^{\cdot} \rightarrow H_2,\\
&H^{\cdot} + O_2 \rightarrow HO_2,\\
&{}^{\cdot}OH + H^{\cdot} \rightarrow H_2O,\\
&{}^{\cdot}OH + {}^{\cdot}OH \rightarrow H_2O_2,
\end{aligned}
$$

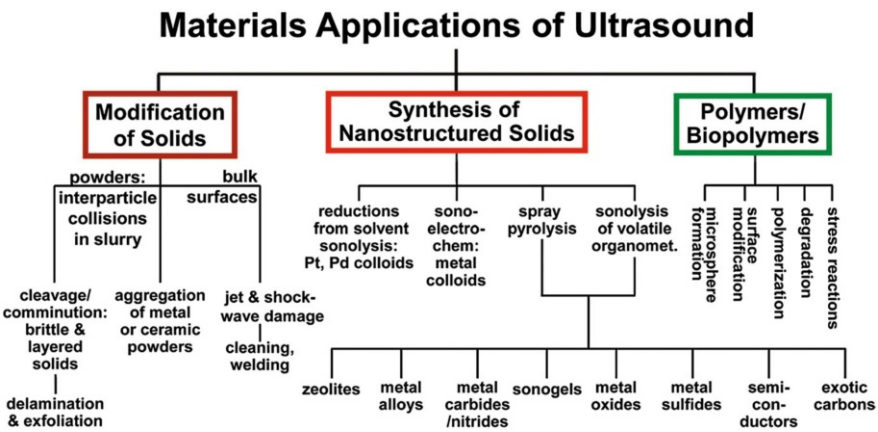

Fig. 3 This chart shows how the various physical and chemical aspects of ultrasound can be used in the production of nanostructured materials. Reproduced with permission from Ref. [1]. Copyright 2012 Royal Society of Chemistry

Thus, during the ultrasonic irradiation of aqueous solutions, both strong oxidants and reductants are formed, and the nature of the overall sonochemical reactions will depend on the conditions. The sonication of nonaqueous liquids also produces radical species [14, 16–18], which can undergo recombination, disproportionation and elimination reactions (e.g., similar to high temperature pyrolysis of hydrocarbons following Rice Radical Chain mechanisms), as well as redox reactions. For example, in the presence of a an organic additive, species like Au(III) can be reduced [19], as discussed in more detail later:

$$RH + {}^{\cdot}OH / H^{\cdot} \rightarrow R^{\cdot} + H_2O / H_2,$$

$$Au(III) + \text{reducing species } (H^{\cdot}, R^{\cdot}) \rightarrow Au(0) \text{ nanoparticles.}$$

2.1 Primary Sonochemistry for Nanoparticle Synthesis

The production of metal nanoparticles from volatile precursors has developed from the first report of amorphous iron nanoparticle synthesis [20]. When a volatile organometallic compound, such as $Fe(CO)_5$, is dissolved in a low vapor pressure alkane solvent or ionic liquid [21, 22] and subjected to intense ultrasound, conditions favor dissociation of multiple metal–ligand bonds, and metal nanoparticles can thus be produced. Due to the short lifetime of a cavitation event, the particle is so rapidly cooled that crystallization is prevented, resulting in amorphous particles. The product appears as an agglomeration of 20-nm nanoparticles (Fig. 4). If oleic acid or a similar surfactant is added to the reaction mixture, colloidal iron nanoparticles 8 nm in diameter are obtained, as shown in the TEM image in Fig. 4 [23]. Using precursor compounds like $Fe(CO)_5$ and $Co(CO)_3NO$, amorphous iron, cobalt and mixed nanoparticles have been made [24].

The synthesis of amorphous metal nanoparticles can be modified by the addition of other reactants to yield a variety of nanomaterials. Addition of sulfur to a solution of $Mo(CO)_6$ and subsequent sonication produces clustered and agglomerated nanoparticles of MoS_2 [25]. This product has a higher edge surface area than conventionally prepared MoS_2, and the catalytic activity is only at the edges where Mo atoms are exposed, not on the flat sulfur faces. MoS_2 is the predominant industrial hydrodesulfurization catalyst, and the sonochemically prepared MoS_2 demonstrates comparatively high catalytic activity for hydrodesulfurization of thiophene as an example. The sonication of $Mo(CO)_6$ [26] and $W(CO)_6$ [27] in an aliphatic solvent produces molybdenum carbide and tungsten carbide, respectively. Sonication of $Mo(CO)_6$ in the presence of air produces MoO_3 nanoparticles. When these precursors are sonicated in the presence of SiO_2 nanoparticles or other inorganic oxide particles, the catalytic material can be directly deposited onto a support during synthesis.

SiO_2 and carbon nanoparticles can also serve as removable templates to metal oxides or sulfides. After the sonochemical production of amorphous iron in the presence of carbon nanoparticles, exposure to air causes the particles to quickly oxidize, forming hollow iron oxide nanocrystals [28]. The crystallization is attributed to the energy generated during the combustion of the carbon nanoparticle template upon air exposure. Figure 5 shows the hollow nature of the resulting hematite nanoparticles. In a control experiment lacking the carbon template,

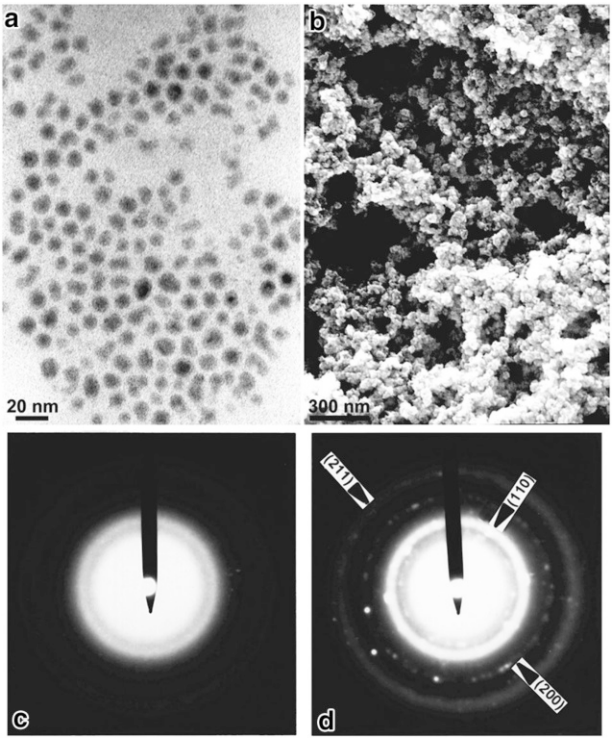

Fig. 4 **a** TEM showing sonochemically produced amorphous iron nanoparticles. **b** SEM of agglomerated amorphous iron nanoparticles. **c** The electron diffraction pattern of the as-produced iron colloid demonstrates its amorphous nature. **d** Heating from the electron beam induces crystallization in situ, as can be seen in the change of the electron diffraction pattern. Reproduced with permission from Ref. [23]. Copyright 1996 American Chemical Society

amorphous iron oxide particles were formed from amorphous iron. Similarly, the sonication of $Mo(CO)_6$ with silica nanoparticles and sulfur or in the presence of air will produce hollow MoS_2 or MoO_3 particles, respectively [29]. An experiment showed the hydrodesulfurization catalytic activity of the sonochemically produced hollow MoS_2 nanospheres outperformed even the non-hollow sonochemically prepared MoS_2. Washing the particles with HF removes the silica, leaving hollow nanoparticles. Annealing the MoO_3 particles forms hollow nanocrystals.

2.2 Secondary Sonochemistry for Nanoparticle Synthesis

Secondary sonochemistry, using a species produced within a cavitating bubble to effect chemical reactions in the liquid phase is widely employed, in part due to its ability to react with nonvolatile species. Even before the mechanisms of sonochemistry were fully understood, Baigent and Müller showed that ultrasound could be used as an alternative to traditional processes for the production of colloidal gold sols [30]. For a detailed discussion of the sonochemical production of metallic nanomaterials, refer to the recent review by Shchukin et al. [4]. Grieser and

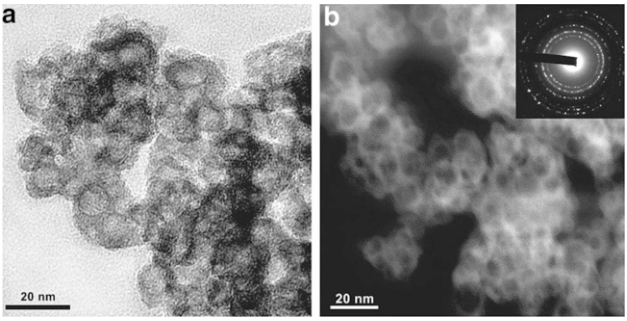

Fig. 5 TEM images of hollow hematite nanoparticles prepared sonochemically from iron pentacarbonyl and carbon nanoparticles in hexadecane. **a** Bright field TEM and **b** dark field TEM images show the nanoparticles and their hollow cores. The *inset* shows the selected-area electron diffraction pattern, demonstrating the crystalline nature of the nanoparticles. Reproduced with permission from Ref. [28]. Copyright 2007 American Chemical Society

coworkers described that when aqueous solutions of $HAuCl_4$ are sonicated in the presence of alcohols or a similar surfactant or organic additive, Au(III) is reduced to Au(0), and gold nanospheres are formed. In a study of the effects of ultrasound frequency on the formation of gold nanoparticles ranging from 20 to 1062 kHz, the fastest rate of Au(III) reduction occurred using 213-kHz radiation [19] in the specific apparatus that they used (which was also the optimized mid-range of the instrument). The size of the gold nanoparticles was also smallest at 213 kHz, as shown in Fig. 6, although the effect on size is rather small compared to the errors in size measurement and may not be statistically significant.

Just as conventional nanoparticle syntheses are able to produce nonspherical nanoparticles, so too can sonochemical syntheses. In the presence of cetyltrimethylammonium bromide and $AgNO_3$, gold nanorods can be formed [31]. Sonochemical nanoparticle synthesis techniques have been used to make gold nanobelts [32], gold nanodecahedra [33], and silver nanoplates [34]. Nie et al. have used the physical effects of acoustic cavitation to create gold nanoparticles with cone-like shapes [35]. In their proposed mechanism, 2-ethoxyanaline, a reductant, is dissolved in hexane. If mixed to with an aqueous gold solution, an emulsion forms. The gold is reduced at the hexane–water interface, forming hemispherical particles. If the phases are emulsified at much lower acoustic power with an ultrasonic bath, however, cone-like particles are made. The authors propose this may due to be a consequence of cavitation bubble collapse, although the exact mechanism is not at all clear; the cone shape may derive instead from larger, irregularly shaped micelles formed from the low acoustic intensities of a cleaning bath.

Ultrasound has been used to produce other noble metal nanoparticles as well. Mizukoshi et al. produced gold–palladium core-shell nanoparticles [36]; Au–Ag [37] and Au–Pt [38] have subsequently been produced as well. The sonochemical production of these core-shell bimetallic nanoparticles is likely in part due to the different reduction potentials for the different metal ions. In the Au–Pd system, the gold is reduced first and the nanoparticles serve as a nucleation site for Pd reduction [36]. Pt–Ru core shell particles were made by sequential sonication of a Pt solution

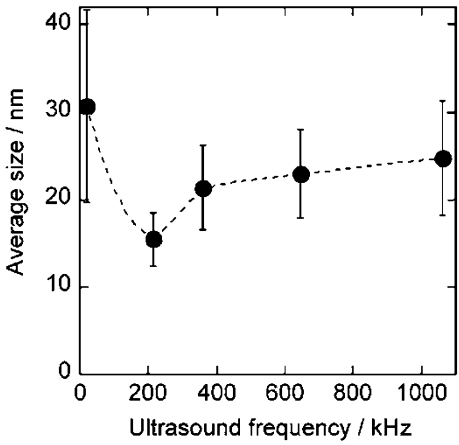

Fig. 6 A graph of gold nanoparticle size as a function of ultrasonic frequency. The particles size is minimized at 213 kHz, which corresponds to the maximum rate of Au(III) reduction observed at the same frequency. Reproduced with permission from Ref. [19]. Copyright 2005 American Chemical Society

followed by a Ru(III) solution in PVP or SDS [13]. Uniform bimetallic nanoparticles have also been produced sonochemically, including $PtCu_3$ [39], PdAg [40], and Pd/first-row transition metal particles [41].

Using poly(methacrylic acid) as a capping agent and hydroxyl radical scavenger, Suslick and coworkers were able to use high-intensity ultrasound to make extremely small (<2 nm) silver nanoclusters [42]. These nanoclusters exhibited a strong fluorescence at 610 nm, unlike larger silver nanoparticles, which do not exhibit fluorescence. Sonochemically produced Ag nanoclusters have been used for the detection of dopamine [43] and sulfide anions [44]. Gold nanoclusters [45] and copper nanoclusters [46] have been produced as well.

Sonochemistry has been employed to synthesize a variety of materials other than noble metals with a variety of structures. Among these materials, various metal oxide and hydroxide nanoparticles have been produced sonochemically, including MgO [47], $Sr(OH)_2$ [48], Dy_2O_3 [49], and Fe_3O_4 [50]. Metal oxides may be formed through sonochemical oxidation via radicals or through sonohydrolysis. Nanostructured zinc oxide is a material of interest as a wide band gap semiconductor, for use as a photocatalyst, and for its antimicrobial properties. Recently, a colloidal suspension of ZnO was produced when zinc acetate was ultrasonically irradiated in a basic solution with a colloidal stabilizer, poly(vinyl alcohol) [51]. The colloidal particles were 10 nm in diameter as determined by dynamic light scattering measurements.

To make a nanostructured ZnO layer as a matrix in an electrochemical sensor, ZnO nanorods and nanoflakes were grown on a Si substrate by sonicating a zinc salt with hexamethylenetetramine, which served as shape directing agent [52]. Similarly, ZnO nanoparticles have been sonochemically produced and simultaneously deposited on a textile surface in an effort to make an antimicrobial surface in a one-step process [53]. Silver [54] and CuO [55] nanoparticles have also been sonochemically formed on textiles and paper surfaces in a similar manner. The specific mechanism by which these nanoparticles inhibit microbial growth is not well understood, although it is well known that these metal ions are toxic to

bacteria. The ease of coating a variety of materials with inorganic nanoparticles using ultrasound may be useful for other applications besides antibacterial activity, such as modifying surface hydrophobicity.

Besides coating bulk textiles materials, sonochemistry can also be used to coat nanostructured surfaces with nanoparticles. Hierarchically structured ZnO microspheres were coated with sonochemically produced CdS nanoparticles as a photosensitizer to make a hierarchical photocatalyst that was more active through the absorbance of visible light than ZnO is alone [56]. While the ZnO was produced through a hydrothermal synthesis, CdS nanoparticles were produced by the sonication of an aqueous solution of cadmium chloride and thiourea with suspended ZnO microspheres. The thiourea was sonochemically reduced to produce sulfide anions, which precipitated with aqueous cadmium to form 50–100-nm spherical CdS nanoparticles (Fig. 7). The interface between the ZnO and the CdS nanoparticles is clean without a buffer zone between the two materials, as the TEM image of Fig. 7c demonstrates. It was suggested that the physical effects of the ultrasound may have a role in cleaning the ZnO surface and providing places for the CdS to nucleate. In photodegradation tests with rhodamine B, the hierarchical ZnO/CdS showed improved activity under solar irradiation than either material alone, which the authors attributed to more efficient charge separation in the composite material.

As with the metal nanoparticles, non-spherical nanoparticles can be made. Examples include ZnO nanorods and triangles [57], as well as SnO_2 nanobelts [58]. One example of this is the formation of Ag/AgCl nanocube plasmonic photocatalysts [59]. By sonicating a solution of silver nitrate, sodium chloride, and poly(vinyl pyrrolidone) in ethylene glycol, uniform nanocubes of AgCl (edge length 115 ± 20 nm) were produced with inclusions of silver nanoparticles, as shown in the SEM images in Fig. 8. The cubic shape was the result of particle growth in the presence of PVP. While the physical effects of the ultrasound helped increased the speed of Oswald ripening in the particles, some of the silver ions in solution were reduced to form silver nanoparticles by the radicals sonochemically generated. Some of these silver nanoparticles became embedded in the AgCl matrices of the nanocubes, giving them a mauve color rather than the usual white of AgCl alone. The Ag/AgCl nanocubes performed photocatalytic degradation of organic dyes better than other reported Ag/AgCl materials.

The ability of sonochemistry to prepare small particles quickly has motivated some research into the sonochemical preparation of porous materials as an alternative to more conventional, and often lengthy, solvothermal synthesis. In a comparative study, Jung and coworkers prepared MOF-177 ($Zn_4O(BTB)_2$, BTB=4,4′,4″-benzene-1,3,5-triyl-tribenzoate) by solvothermal, microwave, and sonochemical methods using 1-methyl-2-pyrrolidone (NMP) as the solvent [60]. Both the microwave and sonochemical syntheses required only an hour to complete, in contrast to the 48 h required by the solvothermal method. Also, the particles produced by microwave and sonochemical methods were smaller than those produced using the conventional synthesis. The BET surface area of the microwave particles was less than that of the sonochemical and conventional particles, which

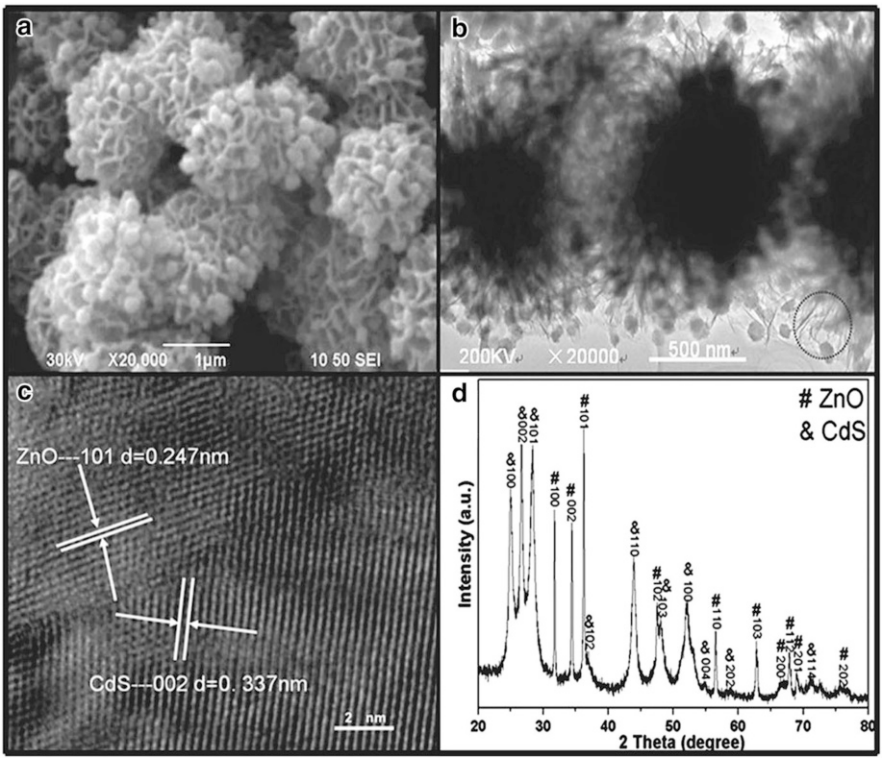

Fig. 7 ZnO/CdS hierarchical heterostructures. **a** SEM image showing CdS nanoparticles incorporated into the porous ZnO structure. **b** TEM of the ZnO/CdS hierarchical heterostructures. **c** High resolution TEM showing the heterojunction between a ZnO nanosheet and a CdS nanoparticle. The interface does not show any buffer layers. **d** Powder XRD pattern of the ZnO/CdS structures includes peaks from both phases. Reproduced with permission from Ref. [56]. Copyright 2012 Royal Society of Chemistry

had similar properties. In a test of CO_2 adsorption, the sonochemical particles exhibited the highest uptake of the three methods.

In another report, a sonochemical method for the preparation of Mg-MOF-74 ($Mg_2(dhtp)(H_2O)_2{\cdot}8H_2O$, dhtp=2,5-dihydroxyterephthalate) was adapted from the conventional solvothermal method [61]. The sonochemical method did not work unless triethylamine was added to the solution to encourage deprotonation of the dhtp. Again, the sonochemical method was able to produce MOF particles with similar BET surface area and performance to the conventional preparation method in a reduced amount of time. The particle morphology differed between the methods. The conventional method produced agglomerated needle 14 μm particles, while the sonochemical method produced spherical 0.6 μm particles. Addition of triethylamine for the solvotothermal method produced particles of intermediate structure and size, showing that this likely has some effect on the particle formation in addition to the ultrasound. The research of Ahn and coworkers has additionally produced sonochemical methods for the preparation of MOF-5 [62], ZIF-8 [63], and

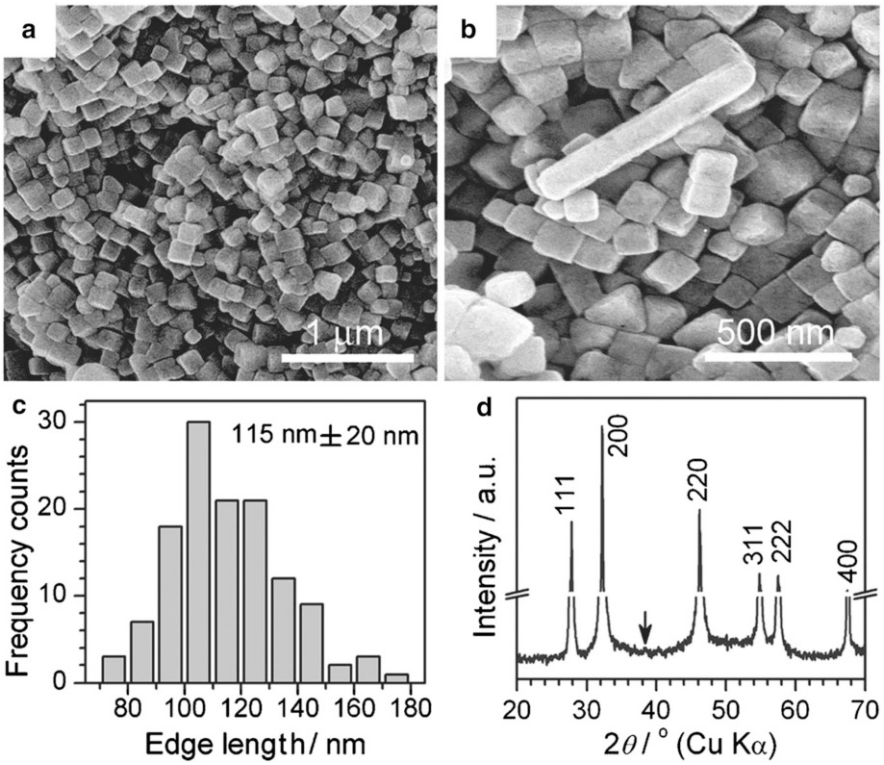

Fig. 8 **a**, **b** SEM images showing the cubic structure of the Ag/AgCL particles. **c** A histogram of the distribution of particle edge lengths. **d** The X-ray diffraction pattern of the Ag/AgCl particles is shown. The peaks match a cubic phase of AgCl, with the corresponding planes labeled. The *arrow* points to a weak peak that matches the Ag(111) plane. Reproduced with permission from Ref. [59]. Copyright 2012 Wiley-VCH Verlag GmbH & Co. KGaA

IRMOF-3 [64]. Other porous materials prepared by ultrasonic methods include manganese dioxide octahedral molecular sieves (OMS) [65].

Sonochemical synthesis of high surface area carbon materials have been of interest as well, as reviewed recently in detail by Skrabalak [66]. Much like the examples mentioned above, efforts have been made to deposit sonochemically produced nanoparticles onto a graphene substrate. Guo et al. prepared 5-nm TiO_2 nanoparticles deposited on graphene sheets by the ultrasonic irradiation of a suspension of graphene oxide with $TiCl_4$ in ethanol, followed by reduction of the graphene oxide [67]. The composite showed improved activity over TiO_2 alone in the photocatalytic degradation of methylene blue. The authors attribute this improvement in part to the ability of the graphene to reduce the recombination of electron-hole pairs. Sonochemistry has been used to couple graphene oxide and graphene to other nanoparticles as well, including Au [68] and Fe_3O_4 [69]. Graphene nanosheets themselves have reportedly been produced from the reduction of graphene oxide via the assistance of ultrasonic irradiation [70]. It was proposed that in addition to dispersing and activating the graphene oxide surface, the radical

species produced during cavitational collapse might also play a role in speeding up the reduction of graphene oxide by hydrazine.

Rather than prepare graphene through the reduction of graphene oxide, Xu and Suslick used sonochemistry to exfoliate graphene from graphite and simultaneously functionalize it with polystyrene to improve its dispersion [71]. Styrene was chosen as a suitable solvent for graphite exfoliation since it has a surface tension of 35 dyn cm^{-1}, which is a good match the surface energy of graphite. Also, under sonochemical conditions, styrene will produce radicals that can chemically attach to the surface of exfoliated graphene sheets and functionalize them, thus improving their dispersibility. This method produced a colloid of single- and few-layered graphene, as shown in the TEM of Fig. 9. The polystyrene-functionalized graphene was soluble in dimethylformamide, tetrahydrofuran, toluene, and chloroform, and the solutions were stable for months without precipitation. Other polymerizable solvents, like 4-vinylpyridine, were also able to produce functionalized graphene.

Sonochemistry has been useful in the synthesis of other carbon nanomaterials as well. Jeong et al. ultrasonically irradiated a suspension of silica powder in *p*-xylene with a small amount of ferrocene to produce single-walled carbon nanotubes (SWCNTs) [72]. The ferrocene decomposed as described above into amorphous iron particles that were able to catalyze the formation of the SWCNTs, and the *p*-xylene was the carbon source. Recently, Ha and Jeong reported the sonochemical formation of multiwalled carbon nanotubes (MWCNTs) as well [73]. The synthesis of MWCNTs was similar to that of SWCNTs but required a higher concentration of ferrocene in the reactant mixture as well as the addition of a small amount of water. With some adjustment, the authors propose this method may be modified to produce fullerenes and carbon onions.

Sonochemistry can also play a role in traditional carbon nanotube syntheses. Sonication is a popular method to disperse individual SWCNTs in solutions. Amide solvents, such as *N*-methyl pyrrolidone (NMP), tend to disperse SWCNTs well. Yau et al. investigated small impurities present when SWCNTs are dispersed in NMP [74]. They found that these impurities could be produced in NMP alone after similar ultrasonic treatment and are likely the result of sonochemical degradation of NMP.

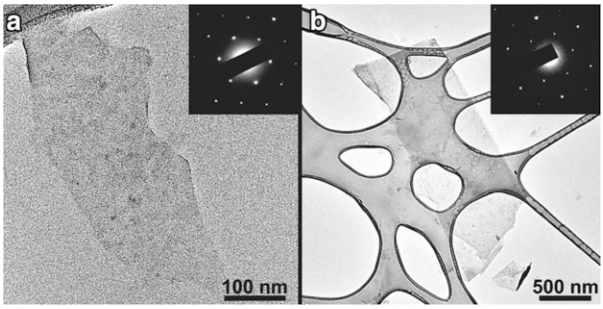

Fig. 9 TEM images showing **a** single-layer and **b** trilayer polystyrene-functionalized graphene prepared sonochemically. The *insets* in each image show the selected area electron diffraction patterns of the graphene samples, confirming the specimen structure. Reproduced with permission from Ref. [71]. Copyright 2011 American Chemical Society

Thermogravimetric analysis of the SWCNTs dispersed in NMP using ultrasound exhibited significant decomposition at 350–500 °C, whereas as-received SWCNT bundles and SWCNTs soaked in NMP without sonication lost only 10% of their mass over the 200–850 °C temperature range. These results suggest that the NMP degradation products adhere to or react with the sonicated SWCNTs, which may be important for their dispersion but detrimental to their thermal stability.

The production of luminescent carbon nanodots (CDs) via ultrasound by Xu et al. is both a further example of another possible carbon material made through sonochemistry as well as an instance where the delineation of primary and secondary sonochemistry becomes ambiguous [75]. The CDs were made from the sonication of an aqueous solution of citric acid as the carbon source and ethylenediamine as an N-doping source, both in rather high concentration (0.5–1 M). Sonication of the solution for 8 h produced 3–7-nm particles, as measured by TEM. X-ray diffraction suggested the particles were amorphous. The CDs had an absorbance band at 354 nm and luminescence at 450 nm when excited with 360-nm light. By optimizing the citric acid/ethylenediamine ratio and concentration, particles with a quantum yield up to 77% were made. This is high in comparison to other reported CD synthesis methods.

Xu et al. observed that the duration of sonication did not have a large impact on the CD quantum yield. If the CDs were formed from secondary reactions in solution, longer sonication should increase particle size and influence luminescence properties. Thus, they proposed that the CDs are formed within the collapsing bubbles. As shown in the diagram in Fig. 10, since citric acid and ethylenediamine are not volatile, they are entering collapsing bubbles via the injection of nanodroplets caused by unstable bubble collapse, as described earlier. In the intense conditions of the collapsing bubble, the droplet solvent evaporates, and the reactants are pyrolyzed to form the CDs. To further test this proposed mechanism, the citric acid was replaced with $M_w = 1800$ Da polyacrylic acid, and CDs were still formed. CDs have also been prepared in other studies using glucose and poly(ethylene glycol) as the carbon source [76].

3 Physical Effects of Ultrasound for Nanoparticle Production

The physical effects of high-intensity ultrasound (microjet formation, turbulence, rapid mixing, shock wave formation, and interparticle collisions in slurries) are also often important in the formation of nanostructured materials. As discussed earlier, cavitational collapse of bubbles generates shock waves that propagate out into the liquid medium. Bubble collapse near a solid surface is non-spherical and causes the formation of microjets that can impact surfaces and eject material out into solution. Turbulent flow and microstreaming make ultrasonic irradiation an effective means to mix liquids, erode solid surfaces, and facilitate interparticle collisions in suspensions of solid particles in liquids [1, 3, 5, 77–79].

This is exemplified by the production of ZnO hierarchically structured microspheres by Wang et al. [80]. They precipitated ZnO from an aqueous solution of $Zn(NO_3)_2$ and NaOH. The ZnO precipitated as interconnected nanosheets,

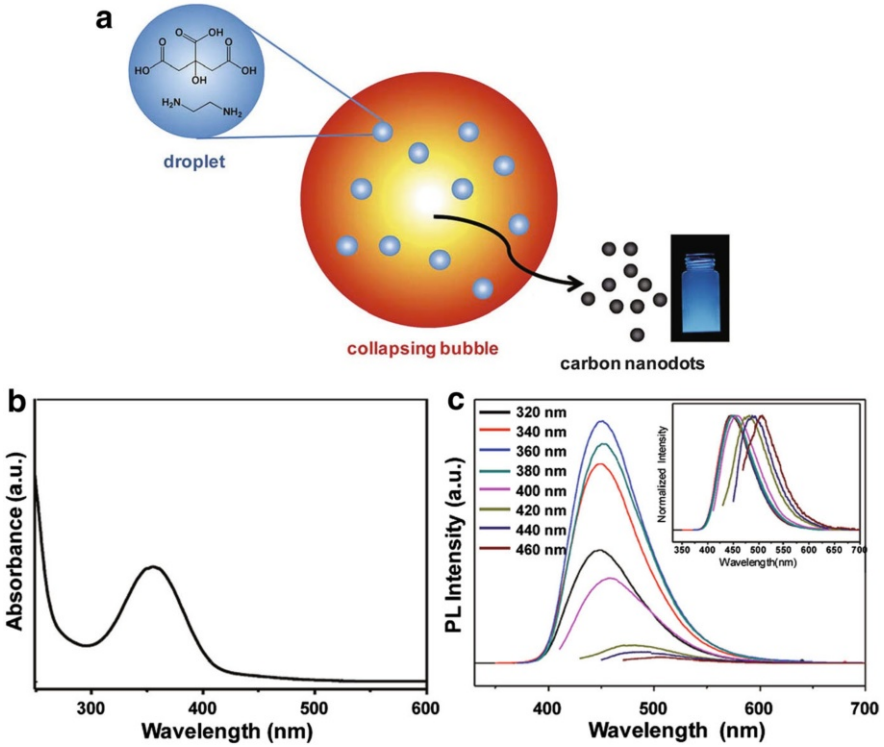

Fig. 10 **a** Schematic diagram of proposed sonochemical synthesis of carbon nanodots from aqueous citric acid. It was proposed that droplets containing citric acid are injected into collapsing cavitation bubbles, where the solvent is quickly evaporated and the citric acid pyrolyzed in the extreme sonochemical conditions, thus forming carbon dots. **b** UV/Vis absorption spectrum and **c** emission spectra of sonochemical carbon dots from various excitation wavelengths. Adapted with permission from Ref. [75]. Copyright 2014 Royal Society of Chemistry

forming flower-like structures. In the absence of ultrasonic irradiation, however, the structures took a longer time to form, were less uniform in size, and exhibited morphology differing from the nanosheets in places. These structures are shown for comparison in Fig. 11. The researchers attribute the structure of the ultrasonically irradiated samples to improved nucleation and diffusion as a result of ultrasound. They hypothesize that the hot spots generated via ultrasound increase the nucleation of the ZnO nanosheets and the shockwaves and microjets improve diffusion and dispersal of nanocrystals. A further experiment of interest would be to precipitate the ZnO while using a high-speed mixer to assess whether improved nucleation through hot spot generation is necessary for the formation of the hierarchical structures or if improved mass transfer suffices.

Similarly, the changes of the size and distribution of ZIF-8 (ZIF = zeolitic imidazolate framework, a Zn^{2+}-imidazolate metal-organic framework) nanoparticles under sonication utilizes the physical effects of ultrasound to alter the structure of nanoparticles [81]. ZIF-8 is prepared through precipitation when methanol

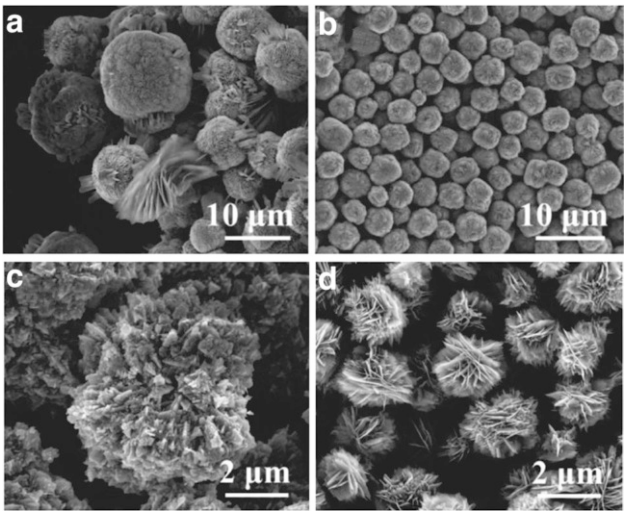

Fig. 11 SEM images demonstrating the effect of ultrasound on the precipitation of ZnO materials. In **a**, **c** ultrasound was not used, resulting in ZnO precipitates that vary widely in size and structure. In contrast, **b**, **d** show ZnO precipitates that were produced with sonication. The particles show a more uniform size distribution and exhibit nanosheet structures at higher magnification (as in **d**). The authors attribute these differences in morphology to the enhanced mixing caused by ultrasound, minimizing local inhomogeneous diffusion and nucleation. Reproduced with permission from Ref. [80]. Copyright 2013 American Chemical Society

solutions of zinc nitrate and 2-methylimidazole are mixed together, making particles about 200 nm in diameter. When these particles are subjected to sonication some particles increase in size while others diminish, resulting in a bimodal distribution. This bimodal distribution is evidence of Ostwald ripening. It is thought that cavitation events near the surface of the nanoparticles help facilitate the dissolution of the smaller particles, and the diffusion of materials in solution is also enhanced by the ultrasound.

3.1 Ultrasonic Spray Pyrolysis for Nanomaterials

Another method that utilizes the physical effects of ultrasound to make nanostructured materials is ultrasonic nebulization (also known as "atomization", which of course it is not!). Ultrasonic irradiation of liquids with sufficient intensity can cause the ejection of liquid droplets from the crests of capillary waves on the liquid surface. The droplets ejected are of a generally uniform size, and the average size can be predicted from the Lang equation [82]:

$$D = 0.34\left(\frac{8\pi\gamma}{\rho f^2}\right)^{1/3},$$

where D is the diameter of the droplet, γ is the surface tension of the liquid, ρ is the liquid density, and f is the frequency of the ultrasonic irradiation. For water nebulized with a 1.65-MHz transducer, the average droplet size is about 3 μm in

diameter. Each droplet is a small, individual chemical reactor that can be flowed through heat, light, or other stimuli to induce chemical reactions. One of the advantages of ultrasonic nebulization is that dense mists can be formed independent of gas flow rate. In addition, it is an easily scaled technique for both laboratory and pilot plant production. By varying reactants, solvent, auxiliary additives, reactor temperature, etc, a variety of different materials with nanostructured morphology can be produced.

Ultrasonic spray pyrolysis (USP) sends an ultrasonically nebulized precursor solution into a carrier gas stream through a heated region, where thermal decomposition can be used to create nano- and micromaterials [2, 3]. A diagram of a typical apparatus used for USP reactions is given in Fig. 12. A more detailed review of the principles and variations of USP has recently appeared [83]. Besides the obvious similarity of both sonochemistry and USP utilizing ultrasound, the two techniques also both restrict reaction zones into sub-micrometer regions—sonochemistry occurs in hot gaseous regions within the cavitation bubble a liquid medium, while USP uses hot liquid droplets isolated in a gas flow. A wide variety of nanostructured materials can be made with ultrasonic spray techniques, such as metals, metal oxides, carbon, semiconductor materials, and polymers.

The simplest forms of particles that USP will form are compact, solid microspheres and hollow shells. Whether solid or hollow particles are made can in part be described by the Peclet number, or the ratio of the solvent evaporation rate to the rate of solute diffusion through the droplet. If solvent evaporation is fast or the material quickly precipitates and forms, hollow shells can be produced. These shells may break apart, forming either a dense agglomeration of particles or small fragments, depending upon the material.

In a recent example of the formation of solid particles by an ultrasonic spray method, Suslick et al. prepared silicone microspheres [84]. The production of polydimethylsiloxane (PDMS) microsphere through emulsion polymerization (the typical method of making polymer microspheres) results in polydisperse particles with large sizes (100 μm) due to the very low surface energy of silicones; other methods that can make small microspheres could only produce particles one at a

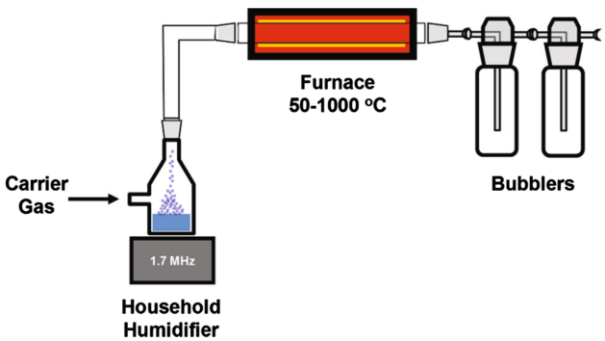

Fig. 12 Simplified diagram of the apparatus used for ultrasonic spray pyrolysis. The household humidifier has a 1.7-MHz ultrasonic transducer to induce nebulization of the reactant solution

time. By generating individual particles through an ultrasonically generated mist, however, microspheres of a uniform size can be readily prepared in quantity. Generally, PDMS oligomers were diluted in hexane or toluene solutions. The mist of this solution was conveyed through a 300 °C tube furnace on an Ar stream, where the solvent evaporated and the PDMS oligomers crosslinked to form solid microspheres <2 μm in diameter with a narrow size distribution. The size of the PDMS microspheres could be controlled by varying the concentration of the precursor solution, as shown in Fig. 13.

In order to explore the potential utility of the PDMS microspheres, several modifications were made to the basic preparation to produce a variety of microspheres. Incorporating Nile red into the precursor solution resulted in fluorescent PDMS microspheres. Even after thorough washing, the dye was still retained within the microspheres and made the microspheres fluorescent. To test whether the microspheres could be used for drug delivery, Rhodamine 6G was used

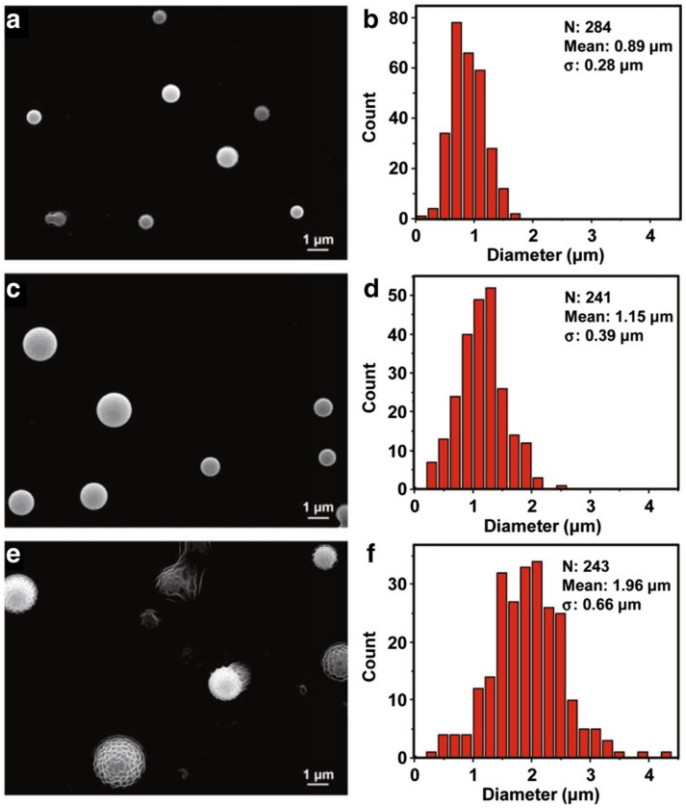

Fig. 13 The size of PDMS (polydimethylsiloxane) microspheres can be controlled by varying the concentration of PDMS in the precursor solution. These SEM images show PDMS microspheres prepared using **a** 4 mg mL^{-1}, **c** 20 mg mL^{-1}, **e** 100 mg mL^{-1} PDMS in hexanes. **b**, **d**, **f** Size distributions of microspheres shown in **a**, **c**, **e**, respectively. Reproduced with permission from Ref. [84]. Copyright 2015 Wiley-VCH Verlag GmbH & Co. KGaA

to assess the loading and release properties of the PDMS microspheres with small hydrophobic molecules. The microspheres exhibited only 25% release after 200 h in phosphate buffered saline, likely due to the inhibition of particle wetting owing to the hydrophobicity of the PDMS. Incorporation of polar side chains or copolymers improved release properties. Magnetic cores could be incorporated into the PDMS microspheres by adding Fe_3O_4 nanoparticles to the precursor solution, which may make PDMS microspheres a possible platform for MRI contrast agents. Cytotoxicity studies showed that PDMS microspheres are not toxic to cells, even at a concentration of 10^5 microspheres/cell.

Suslick and coworkers have used USP to produce hollow microspheres of ZnS:Ni^{2+} [85] and aluminum metal [86]. The hollow ZnS:Ni^{2+} were formed from the removal of a colloidal silica core with HF etching. The segregation of ZnS toward the surface of the microsphere is attributed to low solubility of ZnS and its precursors in the aqueous precursor solution, causing it to precipitate out of solution soon after heating. The thin shell aluminum metal particles were formed by a slightly different mechanism, owing to the reaction of gaseous $TiCl_4$ as a reductant with trimethylamine aluminum hydride at the surface of the nebulized droplets. Conditions can be adjusted to form shells that are nonporous and trap some of the precursor solvent and $TiCl_4$.

Materials made with USP are often porous. Porosity can be produced from the decomposition of the precursors, or it can be introduced through the use of templates. Some porous microspheres produced using aerosol procedures include γ-alumina [87], titania [88], and TiN [89]. The synthesis of MoS_2 by USP exemplifies the use of colloidal silica templates making porous nanostructured microparticles [90]. Microspherical particles were made from an aqueous precursor solution of colloidal silica and $(NH_4)_2MoS_4$. Silica in the microsphere product was etched away with HF, leaving a highly porous MoS_2 microspheres. Highly porous metal oxide particles can also be prepared using USP with template nanoparticles. The use of a colloidal silica template has been used to make porous titania microspheres [91]. When Suslick and coworkers added other transition metals [Co(II), Cr(II), Mn(II), Fe(II), and Ni(II) salts] to the Ti/Si precursor and partially etched the silica, the resulting microspheres had a ball-in-ball structure of a silica sphere within a porous titania shell, shown in Fig. 14.

Besides colloidal silica, other template materials can be used as well to increase the porosity of USP-produced particles. Colloidal polymeric particles, such as polystyrene, have been used in the production of porous silica microspheres. Polystyrene templates can be removed in the heated reaction zone through pyrolysis, thus requiring no additional removal steps after the product is collected. Suslick and Suh used styrene in a sequential heating setup to template worm-like pores into silica microspheres [92]. The styrene polymerized in the first heated zone, then a second hotter zone was used to decompose and remove the template.

Porous carbon microspheres have also been prepared through the use of colloidal silica templates. Lu and coworkers have used a sucrose precursor solution with different types and amounts of silica to produce carbon microspheres with a range of structures [37, 93, 94]. Recently, Choi and coworkers adapted a procedure to produce porous carbon microspheres to include the addition of silicon nanoparticles

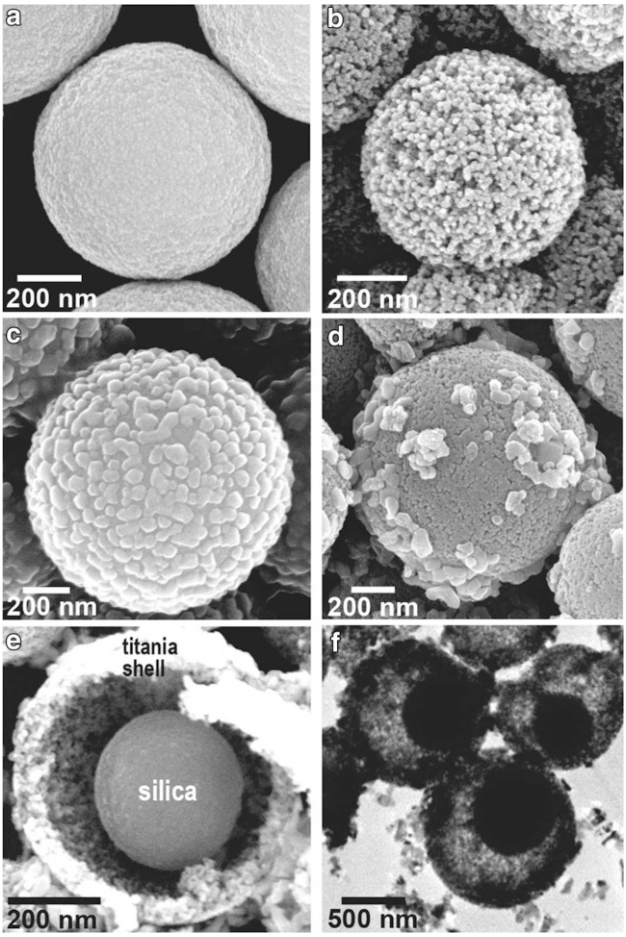

Fig. 14 Electron microscope images of ball-in-ball hollow titania microspheres produced by USP. **a** SEM images of titania and silica microspheres as prepared by USP and **b** after HF etching. **c** SEM of silica and titania microspheres prepared with cobalt shows cobalt oxide particles on the surface of the microsphere, and **d** the microspheres after etching. The ball-in-ball morphology of the etched titania/cobalt oxide microspheres is demonstrated by **e** SEM and **f** TEM. Reproduced with permission from Ref. [91]. Copyright 2006 Wiley-VCH Verlag GmbH & Co. KGaA

[95]. Ultrasonic nebulization of an aqueous sucrose solution containing silicon and silica nanoparticles followed by subsequent pyrolysis and HF etching produced porous carbon microspheres with embedded Si nanoparticles. This composite material was tested as an anode in a lithium ion battery since Si is known to have a large theoretical capacity. The microspheres exhibited high capacity, and retained 91% capacity over 150 cycles. The incorporation of Si nanoparticles in the porous carbon network allowed room for the Si to expand during electrochemical cycling. The coupling of porous carbon for the development of battery electrode materials using USP has also produced microspheres incorporating MoO_3 for lithium ion

batteries [96], sulfur for lithium–sulfur batteries [97], and Na_2FePO_4F for sodium ion batteries [98],

Another templating method is to use precursor materials that form in situ templates upon reaction. For example, porous carbon microspheres have not only been produced through the use of colloidal templates, but also by in situ templates generated by the decomposition of the precursor materials. Porous carbon microspheres have been produced via USP using alkali carboxylates [99] and sucrose [100] as precursor materials. Salts generated by the decomposition of these precursors can act as templates for porosity which are dissolved away upon collection in a suitable solvent. Gaseous products generated by the precursor decomposition may also act as porogens. The nature of the precursor affects the nanostructure of the carbon microspheres. Figure 15 demonstrates the effect of using different alkali metal chloroacetates to produce very different structures in the resulting carbon microspheres.

Despite the production of a variety of porous metal oxides by USP, porous iron oxide had not yet been successfully prepared until recently. Suslick and Overcash were able to produce highly porous iron oxide microspheres using ferritin core analogs (Spiro–Saltman balls) as the precursor material [101]. When the precursor was prepared by mixing $Fe(NO_3)_3$ and Na_2CO_3, porous microspheres with a BET surface area of 301 $m^2\ g^{-1}$ were produced. In contrast, replacing $Fe(NO_3)_3$ with $FeCl_3$ produces hollow porous spheres with a BET surface area of only 97 $m^2\ g^{-1}$. This difference is attributed to the lack of nitrate decomposition, which acts as a

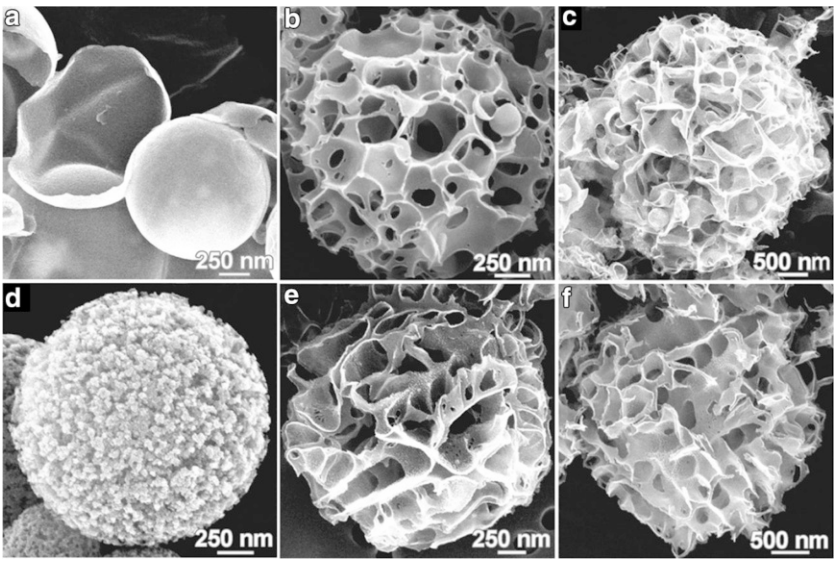

Fig. 15 SEM images of porous carbon microspheres produced by USP. The different morphologies of the microspheres result from the use of different precursor materials: **a** lithium chloroacetate (LiCA), **b** NaCA, **c** KCA, **d** lithium dichloroacetate (LiDCA), **e** NaDCA, and **f** KDCA. Reproduced with permission from Ref. [99]. Copyright 2006 American Chemical Society

porogen during pyrolysis by releasing gases (NO_x) in situ. Mixing the iron salts produced microspheres with intermediate properties.

Suslick and coworkers have also developed porous MnO_2 microspheres for use as a supercapacitor material [102]. Synthesis requires only a precursor solution of $KMnO_4$ and HCl in water. Depending on the reaction temperature, porous or crystalline microspheres could be formed. The different microspheres produced by varying the temperature are shown in the TEM images in Fig. 16. Optimized reaction conditions yielded microspheres which demonstrated a specific capacitance of 320 F g^{-1}. While the microspheres performed best at low charging and discharging rates, coating with poly(3,4-ethlenedioxythiophene) (PEDOT) improved the microsphere performance at higher charge/discharge rates. PEDOT microspheres themselves were also prepared by ultrasonic spray polymerization of a solution of EDOT and an oxidant [103]. The choice of oxidant affected the morphology of the microspheres, yielding either solid, hollow, and porous microspheres. The microspheres had a specific capacitance of 160 Fg^{-1}, which is comparatively high relative to other reports of PEDOT materials.

While generally microspherical morphology predominates the products of USP, Skrabalak and coworkers were able to produce crystalline nanoplates using USP. Through the combination of USP with a molten salt synthesis, $NaInS_2$ nanoplates were prepared [104]. To prepare these nanoplates, $InCl_3$ and excess Na_2S are combined in water and react to form In_2S_3 nanoparticles and dissolved NaCl. Upon nebulization, the droplets are carried by a N_2 stream into a 625 °C furnace. The water evaporates, leaving behind a molten salt flux. Within this flux, $NaInS_2$ crystals

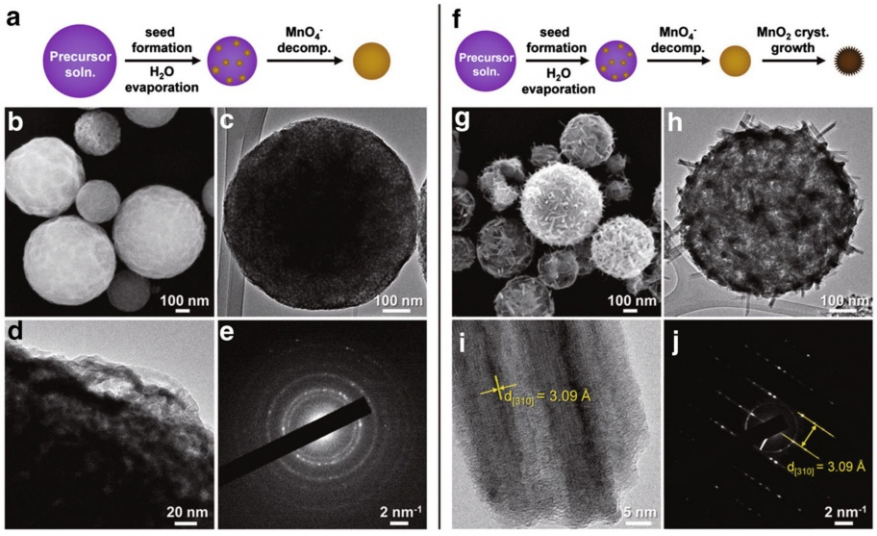

Fig. 16 Morphology of MnO_2 microspheres produced via USP varies according to reaction temperature, as demonstrated by comparison of materials produced at **a**–**e** 150 °C and **f**–**j** 500 °C. As shown in the **c**, **d**, **h**, **i** TEM images, increasing the reaction temperature causes the formation of larger crystals. Also shown are **b**, **g** SEM images, and **e**, **j** electron diffraction patterns. Reproduced with permission from Ref. [102]. Copyright 2015 Wiley-VCH Verlag GmbH & Co. KGaA

nucleate and grow to form hexagonal plates. After collection, the salt flux was removed from the nanoparticles with simple washing, yielding individual single-crystalline nanoplates. Figure 17 shows the $NaInS_2$ plates in comparison to the same material produced through a non-USP method. Without using USP, a similar reaction produced particles without any particular structure or size. The $NaInS_2$ nanoplates were used to construct a photoanode. USP-produced $NaInS_2$ photoanodes outperformed the non-USP samples. The coupling of USP and molten salt syntheses has been used to produce $NaSbO_3$ nanoplates [105], Fe_2O_3 nanoplates, rhombohedra, and octahedra [106], and $CoFe_2O_4$ nanoplates and octahedra [107]. With this technique, scalable flow chemistry can be used to produce unagglomerated, shaped colloidal particles.

The method used by Skrabalak bears similarity to the salt-assisted aerosol decomposition technique developed by Okuyama et al. [108]. This technique involves the production of nanoparticles via USP by preparing single salt or eutectic mixtures of alkali chlorides and nitrates along with the nanoparticle precursor salts so that nanoparticles could nucleate within the molten salt droplet during droplet heating. They reported the synthesis of Y_2O_3–ZrO_2, Ni, Ag–Pd, CdS, ZnS, $LiCoO_2$,

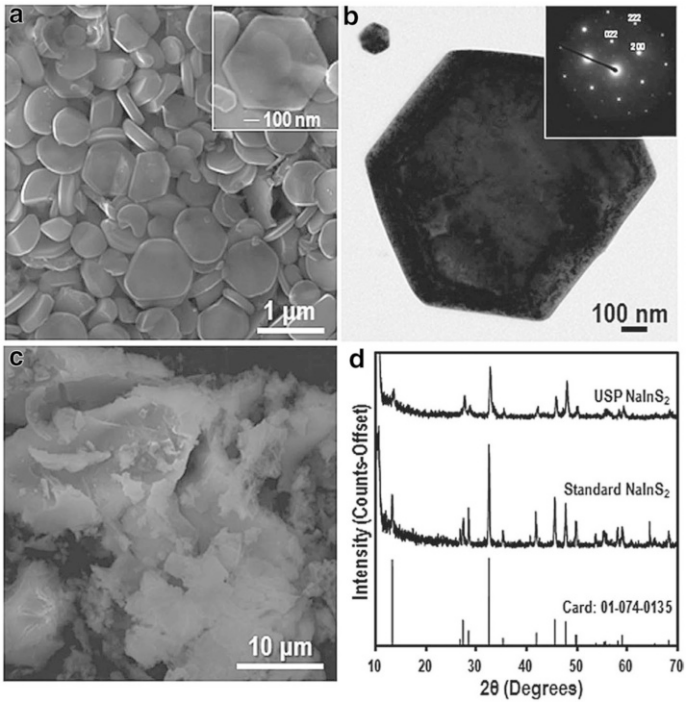

Fig. 17 Comparison of $NaInS_2$ produced by conventional means and molten salt-assisted USP. **a** SEM and **b** TEM images of the nanoplates produced via USP show the hexagonal shape of the nanoplates, and the inset electron diffraction pattern in B demonstrates the single-crystalline nature of the nanoplates. **c** An SEM image of $NaInS_2$ prepared through a non-USP method for comparison. **d** X-ray diffraction patterns of the USP and non-USP materials, as well as a reference for comparison. Reproduced with permission from Ref. [104]. Copyright 2012 Wiley-VCH Verlag GmbH & Co. KGaA

$La_{0.8}Sr_{0.2}Co_{0.5}O_{3-x}$ [108], and CeO_2 [109] nanoparticles using this method, with these nanoparticles exhibiting higher crystallinity than particles produced without the additional salt.

Another similar technique for the production of nanoparticles by USP is chemical aerosol flow synthesis (CAFS), a method developed by Suslick and Didenko [110]. Rather than using salts and aqueous solutions, CAFS is performed with organic solvents. Precursor solutions are prepared with a solvent mixture composed of a high boiling solvent that will served to establish liquid droplets in the heated zone where nanoparticles can form and a low boiling solvent that can dilute the precursor so that it can be nebulized. This method was used to produce semiconducting nanoparticles (i.e., quantum dots) of CdS, CdSe, and CdTe. As a specific example, for the production of ternary CdTeSe quantum dots [111], the Cd and chalcogenide precursors were prepared in octadecene with oleic acid and diluted with toluene. The toluene evaporates as the droplet is heated, and oleic acid-stabilized nanoparticles form in the hot droplets. Particle size could be changed by adjusting the temperature of the tube furnace, giving particles with emissions through the visible region. A blue shift in fluorescence was also observed for the ternary quantum dots due to photo-oxidation, as shown in Fig. 18. The CAFS synthesis of ternary quantum dots allowed emissions to be tuned into the far red and infrared regions as well.

3.2 Sonocrystallization and Sonofragmentation

The application of ultrasound to the preparation of crystalline materials has been an area of interest since the 1950s [112]. Sonocrystallization, using ultrasonic irradiation to aid in the crystallization of materials, is able to produce small crystals of uniform size distribution. The exact means by which ultrasonic irradiation aids in the crystallization of materials is not entirely clear; however, ultrasonic irradiation has been observed to reduce the induction time of crystal nucleation. Also, the width of the metastable zone, the region on a solubility graph between the temperature where equilibrium saturation is reached and the temperature where nucleation is observed, is reduced as well by the use of ultrasound [112]. Bubble collapse may produce areas of increased concentration that may increase the rate of nucleation. Also, the cavitation bubble surface itself may serve as a site for heterogeneous nucleation of crystals. Secondary nucleation can result from the erosion of crystal surfaces during cavitation.

Sonocrystallization has is a promising technique for the pharmaceutical industry. The size and uniform dispersity of pharmaceutical agents can be very important for its intended function, affecting the rate of solubility, how well the material can be delivered, and even its toxicity during use; in other circumstance, control of particle size is critical for efficacious delivery: for example, aerosol delivery of PAs has an optimal particle size, and for parenteral (e.g., intravenous) administration, crystals must be <5 μm to avoid embolisms. Sonocrystallization has been used to prepare crystals of acetylsalicylic acid [113], ibuprofen [114], cloxacillin benzathine [115], and paracetamol [116] in recent studies. For both the ibuprofen and paracetamol studies, sonocrystallization not only produced nano- and microcrystals, but these

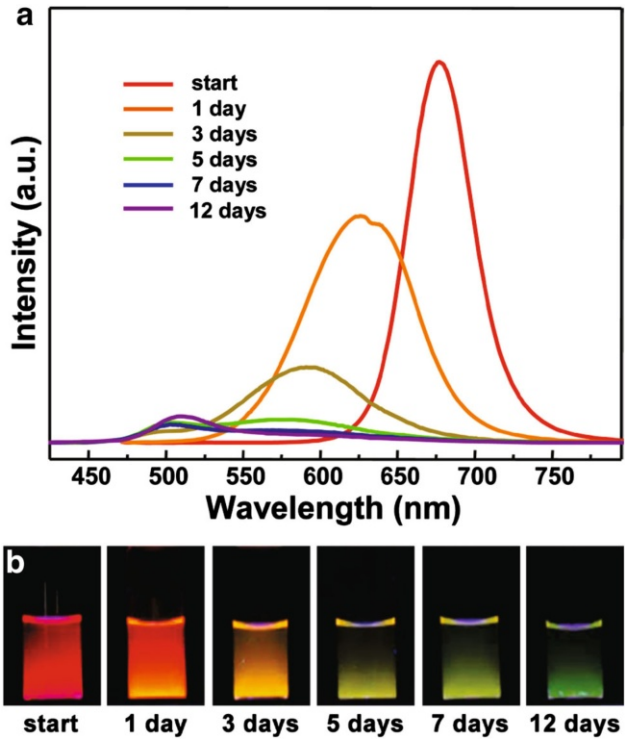

Fig. 18 USP-prepared CdTeSe quantum dots exhibited a blue-shift in fluorescence due to photo-oxidation. The **a** photoluminescence spectra and **b** photographs show the change in fluorescence with time as the CdTeSe quantum dots are exposed to light and air. Reproduced with permission from Ref. [111]. Copyright 2008 American Chemical Society

crystals exhibited better compactibility when forming tablets than conventionally made crystals. The properties responsible for improved compactibility are not entirely clear for either material, although in the case of the ibuprofen the researchers point to slight differences of the powder x-ray diffraction pattern from the reference crystalline material as an indication of possible differences of crystal habit.

Suslick et al. recently developed a spray sonocrystallization method for the preparation of 2-carboxyphenyl salicylate (CPS) [117]. An ethanol solution of CPS was mixed with water, an antisolvent, while passing through a specially prepared ultrasonic horn with a hollowed bore, shown schematically in Fig. 19. This produced well-dispersed crystals with an average size of 91 $\pm$ 5 nm. Crystals were also prepared in the presence of polyvinylpyrrolidone and sodium dodecyl sulfate to improve redispersibility after centrifugation. When ultrasound was replaced by mixing or when crystals were prepared without solvent flow, large crystals or aggregates were produced. Ultrasonic power, antisolvent flow rate, solvent flow rate, and the solvents used did not greatly influence the size of the particles produced by spray sonocrystallization. Only the initial concentration of CPS in the

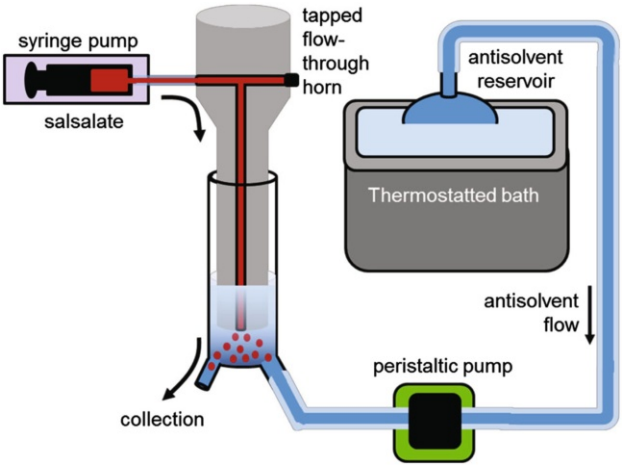

Fig. 19 Schematic diagram showing the apparatus used for spray sonocrystallization. A solution of the material to be crystallized is pumped through a tapped ultrasonic horn into a mixing cell full of a flowing antisolvent. Reproduced with permission from Ref. [117]. Copyright 2015 American Chemical Society

solvent seemed to affect the size of the crystals produced. From this, spray sonocrystallization seems like a robust flow method to produce nanoscale pharmaceutical crystals with a narrow size distribution.

The effects of ultrasound on crystalline materials area not only limited to the nucleation of crystals but also to the fragmentation of crystals in an ultrasonic field. The physical effects of ultrasound on a metal powder suspension were first investigated by Doktycz and Suslick [78] and quantitatively explained by Prozorov and Suslick [79]. Sonication of a slurry of zinc powder in decane produced fused agglomerations of particles. Figure 20 shows an example of two ultrasonically fused Zn particles. Fe, Sn, Cr, and Mo powders also produced fused particles when sonicated, but W powder did not. It was determined that this fusion was the result of interparticle collisions driven by cavitational shock waves.

In contrast to metal particles (which are malleable), the sonication of molecular and ionic crystals (which are friable) as slurries results in fragmentation of the crystals. Suslick et al. conducted a series of experiments to determine the mechanism of sonofragmentation [118]. To test the influence of interparticle collisions, different concentrations of aspirin crystals were suspended in decane and sonicated. Surprisingly, as Fig. 21 shows, it was found that the average particle size after sonication for 10 s did not vary with initial particle concentration, as would have been expected if interparticle collisions were the predominant factor of sonofragmentation. Other experiments were conducted to decouple the horn from the crystal suspension and the suspension from the vessel walls. In both cases, only minimal differences were observed in particle size in comparison to the normally sonicated crystals, ruling out particle–horn and particle–wall interactions as predominating sonofragmentation. These results suggest that shock wave–particle interactions is the major contributor to sonofragmentation.

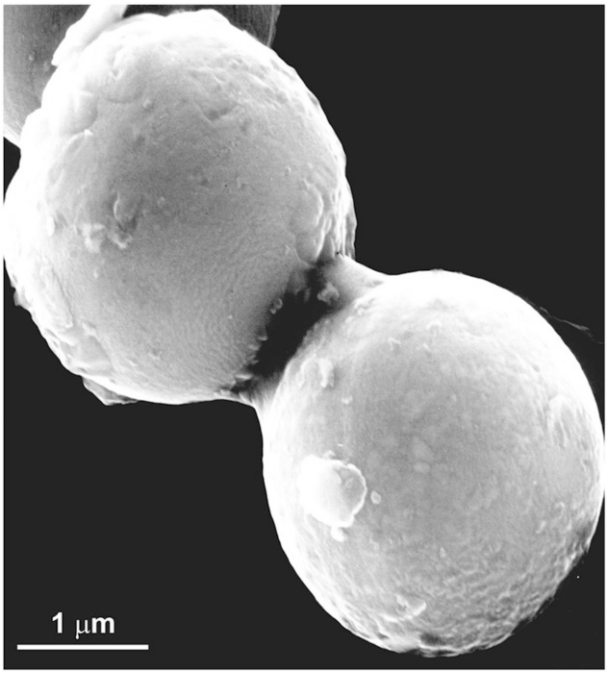

Fig. 20 SEM image showing two fused Zn metal particles. A Zn powder slurry in decane was irradiated with ultrasound, and the resulting shock waves caused interparticle collisions with enough force to fuse the metal particles together. Reproduced with permission from Ref. [78]. Copyright 1990 AAAS

A phenomenon related to sonocrystallization and sonofragmentation is the ability to produce enantiomerically pure crystals from a chiral mixture. Chen and coworkers first reported the growth of $NaClO_3$ crystals consisting predominantly of one enantiomer or the other if a supersaturated solution is ultrasonically irradiated to crystal nucleation and growth [119]. Ultrasonic chiral symmetry breaking in the crystallized portion is thought to be a modified example of Viedma ripening [120], where instead of mechanically grinding the crystals, ultrasound is used to reduce crystal size, i.e., sonofragmentation. In an experimental comparison of deracemization of $NaClO_3$ by ultrasound and by glass bead grinding, Stefanidis et al. subjected racemic suspension of crystals to one of the two methods [121]. The crystals exposed to ultrasound showed a faster initial rate of deracemization, but leveled out before reaching enantiomeric purity. The leveling was attributed to the particles all reaching uniform minimum size. The addition of enantiomerically pure crystals to an ultrasonically irradiated slurry resumed the deracemerization, and enantiomeric purity could be reached in this manner.

Coquerel et al. were able to demonstrate the deracemization of chiral organic crystals [122]. They synthesized a precursor of paclobutrazol, a plant growth inhibitor and fungicide. The prepared crystals were suspended in a methanol–water mixture with NaOH as a racemizing agent for the compound. Experiments were both conducted by mixing the crystal suspensions with glass beads and

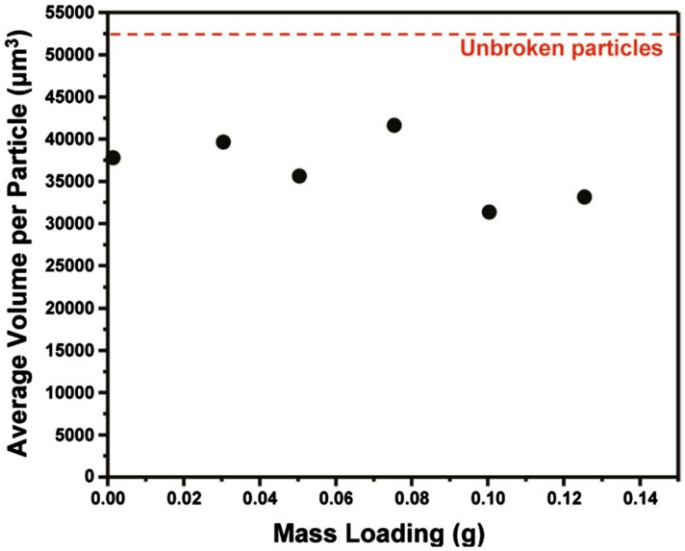

Fig. 21 Graph showing the volume of aspirin crystals as a function of total crystal mass loading as a suspension in dodecane after 10 s of sonication at 5.5 W. The negligible effect of mass loading on the final volume of the crystals is evidence against interparticle collisions as a major contributing mechanism to the sonofragmentation of molecular crystals. Reproduced with permission from Ref. [118]. Copyright 2011 American Chemical Society

ultrasonically irradiating the crystal suspensions. For these crystals, ultrasound was able to completely deracemize samples, and using ultrasound was faster than glass bead abrasion. The rate of deracemization was also found to increase with increasing power of ultrasound applied to the suspensions.

The bulk convection of liquids resulting from cavitation is potentially useful for the self-assembly of colloidal crystals. The formation of colloidal crystals requires a particle to have sufficient energy to move around until it can find a stable configuration relative to the other particles. For small particles, Brownian motion from the thermal energy of the system can drive the self-assembly of colloidal crystals, but larger particles tend to settle due to gravitational effects before a thermodynamically stable configuration can be arranged. Thus, other more complicated methods are usually required to direct the self-assembly of non-Brownian (i.e., larger) particles. The agitation provided by low power ultrasonic irradiation, may serve as an alternative means for larger particles to self-assemble by sedimentation. For example, the use of ultrasonic agitation to facilitate the formation of colloidal crystals was successfully demonstrated by Lash et al. [123]. Ultrasound provides two main advantages in this application. The force exerted by the acoustic waves can counter gravitational effects on particles, allowing the particles to move both macroscopically and microscopically. Second, the convection caused by cavitation also facilitates particle motion and collisions, which enhances the rate at which colloidal crystals form. When the ultrasonic amplitude is optimally set, the particles cluster together in a mechanism similar to inelastic collapse, where collision and

viscous dissipation promote the formation of crystalline structures. Both Brownian and non-Brownian crystals can be formed on the order of minutes.

3.3 Sonochemically Produced Protein Microspheres

The sonochemical production of oil- and gas-filled protein microspheres is an example of both the physical and chemical effects of ultrasound being used to create a nanostructured material [124]. When a mixture of oil and water are irradiated by high-intensity ultrasound, the turbulence generated can produce an emulsion. When an aqueous protein solution is sonicated with an immiscible liquid, protein microspheres are formed. As the oil is emulsified into droplets within the water, proteins attach to the oil–water interface. Meanwhile, cavitation is producing radicals through the sonolysis of water. In the presence of oxygen, superoxide radicals are formed, and these radicals crosslink the proteins through the formation of disulfide bonds. Thus, non-aqueous materials can be encapsulated in a thin, robust protein shell. If an ultrasonic probe is applied to the surface of a protein solution, a thin protein shell can similarly encapsulate gas bubbles [125]. The proteins composing the shell of the microsphere are not denatured by the process of shell formation.

Air- and oil-filled protein microspheres have been greatly studied for possible applications in drug delivery and medical imaging. Gas-filled protein microspheres can be used as a contrast agent for medical sonography [125]. Albunex® and Optison® are commercially available sonographic contrast agents composed of a protein microsphere encapsulating air or octafluoropropane, respectively [126, 127].

Protein microspheres have been used to encapsulate hydrophobic drugs to be used as passive delivery agents [128–130]. Most notably, VivoRx Pharmaceuticals commercialized Abraxane™, albumin microspheres with a paclitaxel core, which is the predominant current delivery system for Taxol chemotherapy for breast cancer [131]; VivoRx became Abraxis Bioscience, which was acquired recently by Celgene for $2.9 billion.

The surface of protein microspheres can be modified post synthesis using layer-by-layer techniques [132]. This technique was used to noncovalently attach peptides made to target integrin proteins overexpressed in some tumor types. The incorporation of gold, carbon, and melanin nanoparticles into the core or shell of the protein microspheres produced contrast agents for optical coherence tomography [133]. The inclusion of dyes or iron oxide nanoparticles in the oil phase produced protein microspheres with fluorescence imaging contrast and MRI contrast, respectively [134].

The sonochemical synthesis of albumin protein microspheres has inspired the use of ultrasound to make microcapsules of different proteins, other biopolymers, and even synthetic polymers. Using ultrasound to produce microspheres does not necessarily need to form covalent crosslinks in order to form somewhat stable microspheres. Biopolymer-stabilized emulsion droplets can be held together by noncovalent interactions (e.g., hydrogen bonding, hydrophobic interactions, and electrostatic interactions) in a manner similar to particle-stabilized pickering emulsions [135]. Avivi and Gedanken were able to produce streptavidin

microspheres despite the fact that streptavidin does not contain cysteine residues. The microspheres did not form under neutral pH but rather in a slightly acidic (pH 6.0) solution, which the authors attributed to hydrophobic interactions stabilizing the microspheres.

Suslick et al. were able to similarly use sodium polyglutamate (SPG) to form microspheres at neutral pH [136]. The presence of added radical scavengers did not affect the formation of the SPG microspheres, and MALDI-MS analysis showed no difference between sonicated and unsonicated SPG, thus showing that covalent bonding did not seem to be responsible in microsphere formation. Rather, hydrogen bonding is an important factor in the stabilization of SPG microspheres. To test whether hydrogen bonding or ion pairing influence microsphere stability, the ionic strength of the SPG solution was adjusted by the addition of $NaNO_3$. Even moderate increases in ionic strength (e.g., adding small 0.1 M $NaNO_3$), which disrupts hydrogen bonding, significantly diminished microsphere stability and formation. Despite the effect of moderate ionic strength on microsphere formation, if microspheres were washed to remove excess counter ions, they were stable when placed in physiological condition buffer solutions, indicating their potential use in medical applications. The robustness of the microspheres was demonstrated by encapsulating and subsequently removing toluene, as shown in Fig. 22. The SPG shell wrinkled like a raisin, but still maintained its integrity.

While polypeptides with and without disulfide crosslinking have been shown to make stable microspheres using ultrasound, there have also been examples of using different biopolymers to sonochemcially form core-shell microspheres. Tzanov and coworkers have made covalently cross-linked nanocapsules using thiolated chitosan [137]. Like the protein microspheres, the thiolated chitosan nanocapsules are stabilized by the formation of disulfide bonds. It was shown that a higher degree of disulfide bond formation could be achieved through increasing the pH of the reactant solution and increasing the degree of chitosan thiolation, resulting in nanocapsules that showed a greater stability against lysozyme degradation. The

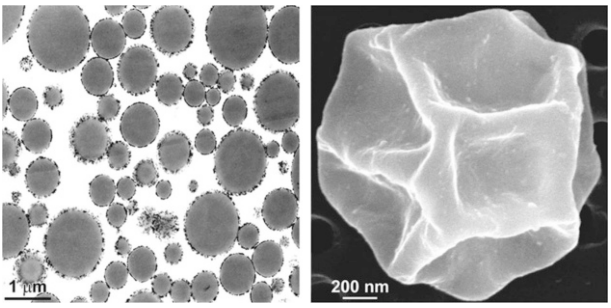

Fig. 22 TEM image (*left*) showing a cross-sectional view of vegetable oil-filled sodium polyglutamate microspheres. SEM image (*right*) of a single sodium polyglutamate microsphere that was prepared using a mixture of toluene and vegetable oil. As the toluene is evacuated, the microsphere contracts, but the shell maintains integrity, demonstrating its robust nature despite the lack of covalent crosslinking. Reproduced with permission from Ref. [136]. Copyright 2006 American Chemical Society

nanocapsules ranged in size from 250 to 570 nm in diameter, depending on the reaction conditions.

Research interest in sonochemically produced protein microcapsules has recently spread to include the remediation of heavy metal-contaminated water [138]. Waters and coworkers tested protein microspheres made from bovine serum albumin and chicken egg white protein, both proteins high in cysteine residues, as a means to remove copper ions from an aqueous solution. This idea was inspired from solvent extraction methods that use air bubble to increase the surface area between the aqueous solution and the extracting solvent. The cysteine residues, which allow for protein crosslinking in the sonochemical production of protein microspheres, should also have the ability to sorb metal ions. Air-filled protein microbubbles were prepared according to the Suslick method, and they were placed in an aqueous solution of copper(II) sulfate. A series of experiments varying temperature, copper concentration, microsphere concentration, and pH were conducted to determine the utility and optimum conditions of protein microbubble metal ion removal. Infrared and X-ray photoelectron spectroscopy of the microbubbles seemed to indicate that thiol, amine, amide, and carboxylate functional groups present on the surface of the microbubbles, and that all were involved in the sorption of copper ions. Under the best conditions tested, 10 g l^{-1} microspheres were able to remove 80% of copper ions from a solution of 1 g l^{-1} copper. Higher loading of microspheres actually resulted in poorer copper removal, possibly due to the formation of microsphere aggregates.

4 Conclusions

High-intensity ultrasound can be a powerful tool for the production of nanostructured materials, in large part stemming from the intense local conditions generated by acoustic cavitation. Such cavitation hot spots can be used to perform chemical reactions that can produce and modify materials. Ultrasound and cavitation also physically affect an irradiated fluid, causing increased mixing and shearing, heating, shock waves, microjets, and droplet nebulization. These processes can affect reaction rates, crystallization, and particle size. This complex variety of chemical and physical effects of ultrasound can be used in a multitude of ways by a discerning chemist, resulting in the wide range of nanostructured materials produced by sonochemical and ultrasound-assisted methods.

References

1. Xu H, Zeiger BW, Suslick KS (2013) Sonochemical synthesis of nanomaterials. Chem Soc Rev 42(7):2555–2567
2. Bang JH, Suslick KS (2010) Applications of ultrasound to the synthesis of nanostructured materials. Adv Mater 22(10):1039–1059
3. Bang JH, Didenko YT, Helmich RJ, Suslick KS (2012) Nanostructured materials through ultrasonic spray pyrolysis. Aldrich Mater Matters 7(2):15–18

4. Shchukin DG, Radziuk D, Möhwald H (2010) Ultrasonic fabrication of metallic nanomaterials and nanoalloys. Annu Rev Mater Res 40(1):345–362
5. Suslick KS, Price GJ (1999) Applications of ultrasound to materials chemistry. Annu Rev Mater Sci 29:295–326. doi:10.1146/annurev.matsci.29.1.295
6. Suslick KS, Flannigan DJ (2008) Inside a collapsing bubble: sonoluminescence and the conditions during cavitation. Annu Rev Phys Chem 59:659–683. doi:10.1146/annurev.physchem.59.032607.093739
7. Didenko YT, McNamara WB, Suslick KS (1999) Hot spot conditions during cavitation in water. J Am Chem Soc 121(24):5817–5818. doi:10.1021/ja9844635
8. Flint EB, Suslick KS (1991) The temperature of cavitation. Science 253(5026):1397–1399. doi:10.1126/science.253.5026.1397
9. Flannigan DJ, Suslick KS (2005) Plasma formation and temperature measurement during single-bubble cavitation. Nature 434(7029):52–55. doi:10.1038/nature03361
10. Didenko YT, Suslick KS (2002) The energy efficiency of formation of photons, radicals and ions during single-bubble cavitation. Nature 418(6896):394–397. doi:10.1038/nature00895
11. Didenko YT, McNamara WB, Suslick KS (2000) Molecular emission from single-bubble sonoluminescence. Nature 407(6806):877–879
12. Xu H, Eddingsaas NC, Suslick KS (2009) Spatial separation of cavitating bubble populations: the nanodroplet injection model. J Am Chem Soc 131(17):6060–6061
13. Ouerhani T, Pflieger R, Ben Massaoud W, Nikitenko SI (2015) Spectroscopy of sonoluminescence and sonochemistry in water saturated with N_2–Ar mixtures. J Phys Chem B 119(52):15885–15891. doi:10.1021/acs.jpcb.5n10221
14. Riesz P, Berdahl D, Christman CL (1985) Free radical generation by ultrasound in aqueous and nonaqueous solutions. Environ Health Perspect 64:233–252
15. Makino K, Mossoba MM, Riesz P (1982) Chemical effects of ultrasound on aqueous solutions. Evidence for hydroxyl and hydrogen free radicals (.cntdot.OH and.cntdot.H) by spin trapping. J Am Chem Soc 104(12):3537–3539
16. Flint EB, Suslick KS (1989) Sonoluminescence from nonaqueous liquids—emission from small molecules. J Am Chem Soc 111(18):6987–6992. doi:10.1021/ja00200a014
17. Suslick KS, Gawienowski JJ, Schubert PF, Wang HH (1983) Alkane sonochemistry. J Phys Chem 87(13):2299–2301. doi:10.1021/j100236a013
18. Suslick KS, Gawienowski JJ, Schubert PF, Wang HH (1984) Sonochemistry in non-aqueous liquids. Ultrasonics 22(1):33–36. doi:10.1016/0041-624x(84)90059-3
19. Okitsu K, Ashokkumar M, Grieser F (2005) Sonochemical synthesis of gold nanoparticles: effects of ultrasound frequency. J Phys Chem B 109(44):20673–20675
20. Suslick KS, Choe SB, Cichowlas AA, Grinstaff MW (1991) Sonochemical synthesis of amorphous iron. Nature 353(6343):414–416
21. Flannigan DJ, Hopkins SD, Suslick KS (2005) Sonochemistry and sonoluminescence in ionic liquids, molten salts, and concentrated electrolyte solutions. J Organomet Chem 690(15):3513–3517. doi:10.1016/j.jorganchem.2005.04.024
22. Oxley JD, Prozorov T, Suslick KS (2003) Sonochemistry and sonoluminescence of room-temperature ionic liquids. J Am Chem Soc 125(37):11138–11139. doi:10.1021/ja029830y
23. Suslick KS, Fang M, Hyeon T (1996) Sonochemical synthesis of iron colloids. J Am Chem Soc 118(47):11960–11961
24. Grinstaff MW, Cichowlas AA, Choe SB, Suslick KS (1992) Effect of cavitation conditions on amorphous metal synthesis. Ultrasonics 30(3):168–172
25. Mdleleni MM, Hyeon T, Suslick KS (1998) Sonochemical synthesis of nanostructured molybdenum sulfide. J Am Chem Soc 120(24):6189–6190
26. Hyeon T, Fang M, Suslick KS (1996) Nanostructured molybdenum carbide: sonochemical synthesis and catalytic properties. J Am Chem Soc 118(23):5492–5493
27. Cau C, Nikitenko SI (2012) Mechanism of W(CO)6 sonolysis in diphenylmethane. Ultrason Sonochem 19(3):498–502
28. Bang JH, Suslick KS (2007) Sonochemical synthesis of nanosized hollow hematite. J Am Chem Soc 129(8):2242–2243
29. Dhas NA, Suslick KS (2005) Sonochemical preparation of hollow nanospheres and hollow nanocrystals. J Am Chem Soc 127(8):2368–2369
30. Baigent CL, Müller G (1980) A colloidal gold prepared with ultrasonics. Experientia 36(4):472–473

31. Okitsu K, Sharyo K, Nishimura R (2009) One-pot synthesis of gold nanorods by ultrasonic irradiation: the effect of pH on the shape of the gold nanorods and nanoparticles. Langmuir 25(14):7786–7790
32. Zhang J, Du J, Han B, Liu Z, Jiang T, Zhang Z (2006) Sonochemical formation of single-crystalline gold nanobelts. Angew Chem Int Edit 45(7):1116–1119
33. Sánchez-Iglesias A, Pastoriza-Santos I, Pérez-Juste J, Rodríguez-González B, García de Abajo FJ, Liz-Marzán LM (2006) Synthesis and optical properties of gold nanodecahedra with size control. Adv Mater 18(19):2529–2534
34. Jiang L-P, Xu S, Zhu J-M, Zhang J-R, Zhu J-J, Chen H-Y (2004) Ultrasonic-assisted synthesis of monodisperse single-crystalline silver nanoplates and gold nanorings. Inorg Chem 43(19):5877–5883
35. Zhang P, He J, Ma X, Gong J, Nie Z (2013) Ultrasound assisted interfacial synthesis of gold nanocones. Chem Commun 49(10):987–989
36. Mizukoshi Y, Fujimoto T, Nagata Y, Oshima R, Maeda Y (2000) Characterization and catalytic activity of core–shell structured gold/palladium bimetallic nanoparticles synthesized by the sonochemical method. J Phys Chem B 104(25):6028–6032
37. Anandan S, Grieser F, Ashokkumar M (2008) Sonochemical synthesis of au–ag core–shell bimetallic nanoparticles. J Phys Chem C 112(39):15102–15105
38. Ataee-Esfahani H, Wang L, Nemoto Y, Yamauchi Y (2010) Synthesis of bimetallic Au@Pt nanoparticles with Au core and nanostructured Pt shell toward highly active electrocatalysts. Chem Mat 22(23):6310–6318
39. Gümeci C, Cearnaigh DU, Casadonte DJ, Korzeniewski C (2013) Synthesis of $PtCu_3$ bimetallic nanoparticles as oxygen reduction catalysts via a sonochemical method. J Mater Chem A 1(6):2322–2329
40. Godínez-García A, Pérez-Robles JF, Martínez-Tejada HV, Solorza-Feria O (2012) Characterization and electrocatalytic properties of sonochemical synthesized PdAg nanoparticles. Mater Chem Phys 134(2–3):1013–1019
41. Matin MA, Jang J-H, Kwon Y-U (2014) PdM nanoparticles (M=Ni Co, Fe, Mn) with high activity and stability in formic acid oxidation synthesized by sonochemical reactions. J Power Sources 262(C):356–363
42. Xu H, Suslick KS (2010) Sonochemical synthesis of highly fluorescent Ag nanoclusters. ACS Nano 4(6):3209–3214
43. Liu T, Zhang L, Song H, Wang Z, Lv Y (2013) Sonochemical synthesis of Ag nanoclusters: electrogenerated chemiluminescence determination of dopamine. Luminescence 28(4):530–535
44. Zhou T, Rong M, Cai Z, Yang CJ, Chen X (2012) Sonochemical synthesis of highly fluorescent glutathione-stabilized Ag nanoclusters and S_2^- sensing. Nanoscale 4(14):4103–4104
45. Li J, Ke CJ, Lin C, Cai ZH, Chen CY, Chang WH (2013) Facile method for gold nanocluster synthesis and fluorescence control using toluene and ultrasound. J Med Biol
46. Wang C, Cheng H, Huang Y, Xu Z, Lin H, Zhang C (2015) Facile sonochemical synthesis of pH-responsive copper nanoclusters for selective and sensitive detection of Pb^{2+}in living cells. Analyst 140(16):5634–5639
47. Alavi MA, Morsali A (2010) Syntheses and characterization of $Mg(OH)_2$ and MgO nanostructures by ultrasonic method. Ultrason Sonochem 17(2):441–446
48. Alavi MA, Morsali A (2010) Syntheses and characterization of $Sr(OH)_2$ and $SrCO_3$ nanostructures by ultrasonic method. Ultrason Sonochem 17(1):132–138
49. Salavati-Niasari M, Javidi J, Davar F (2010) Sonochemical synthesis of $Dy_2(CO_3)_3$ nanoparticles, $Dy(OH)_3$ nanotubes and their conversion to Dy_2O_3 nanoparticles. Ultrason Sonochem 17(5):870–877
50. Ghanbari D, Salavati-Niasari M, Ghasemi-Kooch M (2014) A sonochemical method for synthesis of Fe_3O_4 nanoparticles and thermal stable PVA-based magnetic nanocomposite. J Ind Eng Chem 20(6):3970–3974
51. Nagvenkar AP, Deokar A, Perelshtein I, Gedanken A (2016) A one-step sonochemical synthesis of stable ZnO–PVA nanocolloid as a potential biocidal agent. J Mater Chem B 4(12):2124–2132
52. Vabbina PK, Kaushik A, Pokhrel N, Bhansali S, Pala N (2015) Electrochemical cortisol immunosensors based on sonochemically synthesized zinc oxide 1D nanorods and 2D nanoflakes. Biosens Bioelectron 63(C):124–130
53. Singh G, Joyce EM, Beddow J (2012) Evaluation of antibacterial activity of ZnO nanoparticles coated sonochemically onto textile fabrics. J

54. Gottesman R, Shukla S, Perkas N, Solovyov LA, Nitzan Y, Gedanken A (2011) Sonochemical coating of paper by microbiocidal silver nanoparticles. Langmuir 27(2):720–726
55. Abramova A, Gedanken A, Popov V, Ooi E-H, Mason TJ, Joyce EM, Beddow J, Perelshtein I, Bayazitov V (2013) A sonochemical technology for coating of textiles with antibacterial nanoparticles and equipment for its implementation. Mater Lett 96(C):121–124
56. Xu F, Yuan Y, Han H, Wu D, Gao Z, Jiang K (2012) Synthesis of ZnO/CdS hierarchical heterostructure with enhanced photocatalytic efficiency under nature sunlight. Cryst Eng Comm 14(10):3615–3618
57. Zhang X, Zhao H, Tao X, Zhao Y, Zhang Z (2005) Sonochemical method for the preparation of ZnO nanorods and trigonal-shaped ultrafine particles. Mater Lett 59(14–15):1745–1747
58. Gao T, Wang T (2004) Sonochemical synthesis of SnO_2 nanobelt/CdS nanoparticle core/shell heterostructures. Chem Commun 22:2558–2559
59. Chen D, Yoo SH, Huang Q, Ali G, Cho SO (2012) Sonochemical synthesis of Ag/AgCl nanocubes and their efficient visible-light-driven photocatalytic performance. Chem Eur J 18(17):5192–5200
60. Jung D-W, Yang D-A, Kim J, Kim J, Ahn W-S (2010) Facile synthesis of MOF-177 by a sonochemical method using 1-methyl-2-pyrrolidinone as a solvent. Dalton Trans 39(11):2883–2885
61. Yang D-A, Cho H-Y, Kim J, Yang S-T, Ahn W-S (2012) CO_2 capture and conversion using Mg-MOF-74 prepared by a sonochemical method. Energy Environ Sci 5(4):6465–6473
62. Son W-J, Kim J, Kim J, Ahn W-S (2008) Sonochemical synthesis of MOF-5. Chem Commun 47:6336–6338
63. Lee Y-R, Jang M-S, Cho H-Y, Kwon H-J, Kim S, Ahn W-S (2015) ZIF-8: a comparison of synthesis methods. Chem Eng J 271(C):276–280
64. Lee Y-R, Cho S-M, Ahn W-S, Lee C-H, Lee K-H, Cho W-S (2015) Facile synthesis of an IRMOF-3 membrane on porous Al_2O_3 substrate via a sonochemical route. Microporous Mesoporous Mater 213(C):161–168
65. Dharmarathna S, King'ondu CK, Pedrick W, Pahalagedara L, Suib SL (2012) Direct sonochemical synthesis of manganese octahedral molecular sieve (OMS-2) nanomaterials using cosolvent systems, their characterization, and catalytic applications. Chem Mat 24(4):705–712
66. Skrabalak SE (2009) Ultrasound-assisted synthesis of carbon materials. Phys Chem Chem Phys 11(25):4930–4942
67. Guo J, Zhu S, Chen Z, Li Y, Yu Z, Liu Q, Li J, Feng C, Zhang D (2011) Sonochemical synthesis of TiO_2 nanoparticles on graphene for use as photocatalyst. Ultrason Sonochem 18(5):1082–1090
68. Cui Y, Zhou D, Sui Z, Han B (2014) Sonochemical synthesis of graphene oxide-wrapped gold nanoparticles hybrid materials: visible light photocatalytic activity. Chin J Chem 33(1):119–124
69. Zhu S, Guo J, Dong J, Cui Z, Lu T, Zhu C, Zhang D, Ma J (2013) Sonochemical fabrication of Fe_3O_4 nanoparticles on reduced graphene oxide for biosensors. Ultrason Sonochem 20(3):872–880
70. Krishnamoorthy K, Kim G-S, Kim SJ (2013) Graphene nanosheets: ultrasound assisted synthesis and characterization. Ultrason Sonochem 20(2):644–649
71. Xu H, Suslick KS (2011) Sonochemical preparation of functionalized graphenes. J Am Chem Soc 133(24):9148–9151
72. Jeong S-H, Ko J-H, Park J-B, Park W (2004) A sonochemical route to single-walled carbon nanotubes under ambient conditions. J Am Chem Soc 126(49):15982–15983
73. Ha H, Jeong S-H (2016) Facile route to multi-walled carbon nanotubes under ambient conditions. Korean J Chem Eng 33(2):401–404
74. Yau HC, Bayazit MK, Steinke JHG, Shaffer MSP (2015) Sonochemical degradation of *N*-methylpyrrolidone and its influence on single walled carbon nanotube dispersion. Chem Commun 51(93):16621–16624
75. Wei K, Li J, Ge Z, You Y, Xu H (2014) Sonochemical synthesis of highly photoluminescent carbon nanodots. RSC Adv 4:52230–52234
76. Kumar VB, Ze Porat, Gedanken A (2016) Facile one-step sonochemical synthesis of ultrafine and stable fluorescent C-dots. Ultrason Sonochem 28:367–375. doi:10.1016/j.ultsonch.2015.08.005
77. Suslick KS (1990) Sonochemistry. Science 247(4949):1439–1445. doi:10.1126/science.247.4949.1439
78. Doktycz SJ, Suslick KS (1990) Interparticle collisions driven by ultrasound. Science 247(4946):1067–1069
79. Prozorov T, Prozorov R, Suslick KS (2004) High velocity interparticle collisions driven by ultrasound. J Am Chem Soc 126(43):13890–13891. doi:10.1021/ja049493o

80. Shi Y, Zhu C, Wang L, Zhao C, Li W, Fung KK, Ma T, Hagfeldt A, Wang N (2013) Ultrarapid sonochemical synthesis of ZnO hierarchical structures: from fundamental research to high efficiencies up to 6.42% for quasi-solid dye-sensitized solar cells. Chem Mat 25(6):1000–1012
81. Thompson JA, Chapman KW, Koros WJ, Jones CW, Nair S (2012) Sonication-induced Ostwald ripening of ZIF-8 nanoparticles and formation of ZIF-8/polymer composite membranes. Microporous Mesoporous Mater 158(C):292–299
82. Lang RJ (1962) Ultrasonic atomization of liquids. J Acoust Soc Am 34(1):6
83. Mwakikunga BW (2014) Progress in ultrasonic spray pyrolysis for condensed matter sciences developed from ultrasonic nebulization theories since Michael Faraday. Crit Rev Solid State Mat Sci 39(1):46–80. doi:10.1080/10408436.2012.687359
84. Rankin JM, Neelakantan NK, Lundberg KE, Grzincic EM, Murphy CJ, Suslick KS (2015) Magnetic, fluorescent, and copolymeric silicone microspheres. Adv Sci 2 (6)
85. Bang JH, Hehnich RJ, Suslick KS (2008) Nanostructured ZnS:Ni^{2+} photocatalysts prepared by ultrasonic spray pyrolysis. Adv Mater 20(13):2599. doi:10.1002/adma.200703188
86. Helmich RJ, Suslick KS (2010) Chemical aerosol flow synthesis of hollow metallic aluminum particles. Chem Mat 22(17):4835–4837. doi:10.1021/cm101342r
87. Boissière C, Nicole L, Gervais C, Babonneau F, Antonietti M, Amenitsch H, Sanchez C, Grosso D (2006) Nanocrystalline mesoporous γ-alumina powders "UPMC1 Material" gathers thermal and chemical stability with high surface area. Chem Mat 18(22):5238–5243
88. Li L, Tsung CK, Yang Z, Stucky GD, Sun LD, Wang JF, Yan CH (2008) Rare-earth-doped nanocrystalline titania microspheres emitting luminescence via energy transfer. Adv Mater 20(5):903–908
89. Bang JH, Suslick KS (2009) Dual templating synthesis of mesoporous titanium nitride microspheres. Adv Mater 21(31):3186–3190
90. Skrabalak SE, Suslick KS (2005) Porous MoS_2 synthesized by ultrasonic spray pyrolysis. J Am Chem Soc 127(28):9990–9991. doi:10.1021/ja051654g
91. Suh WH, Jang AR, Suh YH, Suslick KS (2006) Porous, hollow, and ball-in-ball metal oxide microspheres: preparation, endocytosis, and cytotoxicity. Adv Mater 18(14):1832–1837
92. Suh WH, Suslick KS (2005) Magnetic and porous nanospheres from ultrasonic spray pyrolysis. J Am Chem Soc 127(34):12007–12010. doi:10.1021/ja050693p
93. Hampsey JE, Hu Q, Rice L, Pang J, Wu Z, Lu Y (2005) A general approach towards hierarchical porous carbon particles. Chem Commun 28:3606–3608
94. Hu Q, Lu Y, Meisner GP (2008) Preparation of nanoporous carbon particles and their cryogenic hydrogen storage capacities. J Phys Chem C 112(5):1516–1523
95. Jung DS, Hwang TH, Park SB, Choi JW (2013) Spray drying method for large-scale and high-performance silicon negative electrodes in Li–ion batteries. Nano Lett 13(5):2092–2097
96. Ko YN, Park SB, Jung KY, Kang YC (2013) One-pot facile synthesis of Ant-cave-structured metal oxide-carbon Microballs by continuous process for use as anode materials in Li-Ion batteries. Nano Lett 13(11):5462–5466. doi:10.1021/nl4030352
97. Jung DS, Hwang TH, Lee JH, Koo HY, Shakoor RA, Kahraman R, Jo YN, Park M-S, Choi JW (2014) Hierarchical porous carbon by ultrasonic spray pyrolysis yields stable cycling in lithium-sulfur battery. Nano Lett 14(8):4418–4425
98. Langrock A, Xu Y, Liu Y, Ehrman S, Manivannan A, Wang C (2013) Carbon coated hollow Na_2FePO_4F spheres for Na–ion battery cathodes. J Power Sourc 223(C):62–67
99. Skrabalak SE, Suslick KS (2006) Porous carbon powders prepared by ultrasonic spray pyrolysis. J Am Chem Soc 128(39):12642–12643
100. Fortunato ME, Rostam-Abadi M, Suslick KS (2010) Nanostructured carbons prepared by ultrasonic spray pyrolysis. Chem Mat 22(5):1610–1612. doi:10.1021/cm100075j
101. Overcash JW, Suslick KS (2015) High surface area iron oxide microspheres via ultrasonic spray pyrolysis of ferritin core analogues. Chem Mat 27(10):3564–3567
102. Zhang Y, Huff LA, Gewirth AA, Suslick KS (2015) Synthesis of manganese oxide microspheres by ultrasonic spray pyrolysis and their application as supercapacitors. Part Part Syst Charact 32(9):899–906
103. Zhang Y, Suslick KS (2015) Synthesis of poly(3,4-ethylenedioxythiophene) microspheres by ultrasonic spray polymerization (USPo). Chem Mat 27(22):7559–7563
104. Mann AKP, Wicker S, Skrabalak SE (2012) Aerosol-assisted molten salt synthesis of $NaInS_2$ nanoplates for use as a new photoanode material. Adv Mater 24(46):6186–6191. doi:10.1002/adma.201202299

105. Chen DP, Bowers W, Skrabalak SE (2015) Aerosol-assisted combustion synthesis of single-crystalline $NaSbO_3$ nanoplates: a topotactic template for ilmenite $AgSbO_3$. Chem Mat 27(1):174–180
106. Mann AKP, Fu J, DeSantis CJ, Skrabalak SE (2013) Spatial and temporal confinement of salt fluxes for the shape-controlled synthesis of Fe_2O_3 nanocrystals. Chem Mat 25(9):1549–1555. doi:10.1021/cm3038087
107. Fu J, DeSantis CJ, Weiner RG, Skrabalak SE (2015) Aerosol-assisted synthesis of shape-controlled $CoFe_2O_4$: topotactic versus direct melt crystallization. Chem Mat 27(5):1863–1868
108. Xia B, Lenggoro IW, Okuyama K (2001) Novel route to nanoparticle synthesis by salt-assisted aerosol decomposition. Adv Mater 13(20):1579–1582
109. Xia B, Lenggoro IW, Okuyama K (2001) Synthesis of CeO_2 nanoparticles by salt-assisted ultrasonic aerosol decomposition. J Mater Chem 11(12):2925–2927
110. Didenko YT, Suslick KS (2005) Chemical aerosol flow synthesis of semiconductor nanoparticles. J Am Chem Soc 127(35):12196–12197
111. Bang JH, Suh WH, Suslick KS (2008) Quantum dots from chemical aerosol flow synthesis: preparation, characterization, and cellular imaging. Chem Mat 20(12):4033–4038. doi:10.1021/cm800453t
112. Sander JRG, Zeiger BW, Suslick KS (2014) Sonocrystallization and sonofragmentation. Ultrason Sonochem 21(6):1908–1915
113. Eder RJP, Schrank S, Besenhard MO, Roblegg E, Gruber-Woelfler H, Khinast JG (2012) Continuous sonocrystallization of acetylsalicylic acid (ASA): control of crystal size. Cryst Growth Des 12(10):4733–4738
114. Manish M, Harshal J, Anant P (2005) Melt sonocrystallization of ibuprofen: effect on crystal properties. Eur J Pharm Sci 25(1):41–48
115. Li J, Bao Y, Wang J (2013) Effects of sonocrystallization on the crystal size distribution of cloxacillin benzathine crystals. Chem Eng Technol 36(8):1341–1346
116. Bučar D-K, Elliott JA, Eddleston MD, Cockcroft JK, Jones W (2014) Sonocrystallization yields monoclinic paracetamol with significantly improved compaction behavior. Angew Chem Int Ed 54(1):249–253
117. Kim HN, Sander JRG, Zeiger BW, Suslick KS (2015) Spray sonocrystallization. Cryst Growth Des 15(4):1564–1567
118. Zeiger BW, Suslick KS (2011) Sonofragmentation of molecular crystals. J Am Chem Soc 133(37):14530–14533
119. Song Y, Chen W, Chen X (2008) Ultrasonic field induced chiral symmetry breaking of $NaClO_3$ crystallization. Cryst Growth Des 8(5):1448–1450
120. Viedma C (2005) Chiral symmetry breaking during crystallization: complete chiral purity induced by nonlinear autocatalysis and recycling. Phys Rev Lett 94(6):065504
121. Xiouras C, Van Aeken J, Panis J, Ter Horst JH, Van Gerven T, Stefanidis GD (2015) Attrition-enhanced deracemization of $NaClO_3$: comparison between ultrasonic and abrasive grinding. Cryst Growth Des 15(11):5476–5484
122. Rougeot C, Guillen F, Plaquevent J-C, Coquerel G (2015) Ultrasound-enhanced deracemization: toward the existence of agonist effects in the interpretation of spontaneous symmetry breaking. Cryst Growth Des 15(5):2151–2155
123. Lash MH, Fedorchak MV, Little SR, McCarthy JJ (2015) Fabrication and characterization of non-Brownian particle-based crystals. Langmuir 31(3):898–905
124. Suslick KS, Grinstaff MW (1990) Protein microencapsulation of nonaqueous liquids. J Am Chem Soc 112(21):7807–7809
125. Grinstaff MW, Suslick KS (1991) Air-filled proteinaceous microbubbles—synthesis of an echo-contrast agent. Proc Natl Acad Sci USA 88(17):7708–7710. doi:10.1073/pnas.88.17.7708
126. Quay SC (2004) Ultrasound contrast agents including protein stabilized microspheres of perfluoropropane, perfluorobutane, or perfluoropentane. US 6,723,303
127. Kiessling F, Huppert J, Palmowski M (2009) Functional and molecular ultrasound imaging: concepts and contrast agents. Curr Med Chem 16(5):627–642
128. Grinstaff MW, Soon-Shiong P, Wong M, Sandford PA, Suslick KS, Desai NP (1997) Methods for the preparation of pharmaceutically active agents for in vivo delivery. US 5665382
129. Soon-Shiong P, Desai NP, Grinstaff MW, Sandford PA, Suslick KS (1996) Methods for in vivo delivery of substantially water insoluble pharmacologically active agents and compositions useful therefor. US 5560933

130. Grinstaff MW, Soon-Shiong P, Wong M, Sandford PA, Suslick KS, Desai NP (1996) Composition useful for in vivo delivery of biologics and methods employing same. US 5498421
131. Hawkins MJ, Soon-Shiong P, Desai N (2008) Protein nanoparticles as drug carriers in clinical medicine. Adv Drug Deliv Rev 60(8):876–885. doi:10.1016/j.addr.2007.08.044
132. Toublan FJ-J, Boppart S, Suslick KS (2006) Tumor targeting by surface-modified protein microspheres. J Am Chem Soc 128(11):3472–3473
133. Lee TM, Oldenburg AL, Sitafalwalla S, Marks DL, Luo W, Toublan FJ-J, Suslick KS, Boppart SA (2003) Engineered microsphere contrast agents for optical coherence tomography. Opt Lett 28(17):1546–1548
134. John R, Nguyen FT, Kolbeck KJ, Chaney EJ, Marjanovic M, Suslick KS, Boppart SA (2011) Targeted multifunctional multimodal protein-shell microspheres as cancer imaging contrast agents. Mol Imaging Biol 14(1):17–24
135. Avivi S, Gedanken A (2002) S–S bonds are not required for the sonochemical formation of proteinaceous microspheres: the case of streptavidin. Biochem J 366(Pt 3):705–707
136. Dibbern EM, Toublan FJJ, Suslick KS (2006) Formation and characterization of polyglutamate core-shell microspheres. J Am Chem Soc 128(20):6540–6541. doi:10.1021/ja058198g
137. Francesko A, Fernandes MM, Perelshtein I, Benisvy-Aharonovich E, Gedanken A, Tzanov T (2014) One-step sonochemical preparation of redox-responsive nanocapsules for glutathione mediated RNA release. J Mater Chem B 2:6020–6029
138. Nazari AM, Cox PW, Waters KE (2014) Copper ion removal from dilute solutions using ultrasonically synthesised BSA- and EWP-coated air bubbles. Sep Purif Technol 132(C):218–225